Universiteit Leiden

Master Computer Science

FESD: A Fault Estimation Pipeline for Human Pose Estimation

Name:	Leonardo Benedikt Pohl
Student ID:	s3059030
Date:	30/05/2023
Specialisation:	Advanced Computing and Systems
1st supervisor:	Dr. Erwin Bakker
2nd supervisor:	Prof. Dr. Michael Lew

Master's Thesis in Computer Science

Leiden Institute of Advanced Computer Science (LIACS)
Leiden University
Niels Bohrweg 1
2333 CA Leiden
The Netherlands

Abstract

Human pose estimation(HPE), or skeleton detection, has been a topic of research for many years. With the advancement of hardware, it has become viable to apply HPE in real-time applications such as games. However, HPE is a difficult task that is prone to errors or faults, especially in complicated situations, such as cramped environments. These errors might cause human-computer interaction to be hampered.

The goal of this thesis is to (1) understand what causes the problems, and (2) to design exercises which deliberately cause common errors and (3) to capture them within a dataset and label the entries accordingly. Finally, (4) preliminary models are developed to detect the errors or faults caused by HPE using the dataset.

In the scope of this thesis, a method is developed that is capable of capturing and labelling multi-modal data, **F**ault **E**stimator for **S**keleton **D**etection **Data** processor (FESDData). Four different problem sets are defined with increasingly detailed areas, ranging from body-wise fault estimation to joint-wise fault estimation. Using the captured dataset, FESDDataset, preliminary experiments were run. For the preliminary experiments multiple models were developed one model for each of the problem sets, which aim to detect if an error occurs at different levels, **F**ault **E**stimator for **S**keleton **D**etection **Model** (FESDModelv1 and FESDModelv2). While version one of the models uses custom feature extraction the second version uses transfer learning using EfficientNetv2.

In this thesis, common error sources that occur during HPE are found. Based on these error sources, exercises are derived which are captured in the FESDDataset using the dataset collection tool FESDData. The joints of the poses are then labelled based on the errors that occur. I abstract the data to form four different problem sets. For each of the problem sets, two models FESDModelv1 and FESDModelv2, are trained. The results of the preliminary experiments showed that FESDModelv1 outperforms FESDModelv2. Furthermore, from the four defined problem sets, both versions of the model perform best on the half-body problem set. In particular, the best results were achieved when considering the lower body. However, with further research and data FESDModelv1 and FESDModelv2 could be improved.

In conclusion, the preliminary models showed that the data captured by FESDData can successfully be used to create a model for fault estimation for skeleton detection.

Acknowledgement

I would like to thank my supervisor Dr. Erwin Bakker, who guided me throughout this thesis and allowed me to use a depth camera for the thesis. I would like to thank SilverFit for giving me the necessary insight into common errors in HPE, and for allowing me to use their hardware for the collection of the dataset. Additionally, I would like to thank my friends and family who have been patient enough to listen to me talk about my thesis for the past 14 months. And I would especially like to thank my partner Maria Xiberras, who has supported me throughout this thesis, even if that meant many restless weekends and delaying our plans for longer than expected.

Contents

1 Introduction **1**

2 Related Work **3**

3 Fundamentals **5**
3.1 Human pose estimation 5
3.2 Convolutional Neural Networks 7
3.3 Evaluation metrics 7

4 FESDData **11**
4.1 Challenges in HPE 11
4.2 Data acquisition 20
4.3 Data layout 20
4.4 Data labeling 21
4.5 Problem Sets 21
4.6 Recording Setup 22
4.7 Dataset Analysis 23

5 FESDModel **27**
5.1 Model architecture 27
5.2 Data preparation 31
5.3 Experimental Setup 33

6 Results **35**
6.1 FESDModelv1 Results 35
6.2 FESDModelv2 Results 40

7 Conclusion **45**
7.1 Contribution 46
7.2 Future work 46

References **51**

A FESDData Appendix 1 **53**

B FESDData Appendix 1 **55**

C Additional Results for FESDModelv1 **61**

List of Figures

3-1 Different representations of the human pose 6
3-2 An interpretation of the ROC Curve 8

4-1 Trivial Exercises 15
4-2 Easy Exercises 16
4-3 Medium Exercises 18
4-4 Difficult Exercises 19
4-5 FESDData user interface 20
4-6 Visualisation of the Problemsets 22
4-7 Error Distribution of the Full Body 23
4-8 Error Distribution by Body Half 24
4-9 Error Distribution by Body part 24
4-10 Error Distribution for each error class 25

5-1 FESDModel architecture version 1 28
5-2 FESDModel architecture version 2 29
5-3 Network comparison 30
5-4 Data preparation pipeline for FESDModel 32

6-1 Confusion Matrices of FESDModelv1 36
6-2 ROC Curves of FESDModelv1 37
6-3 Confusion matrix of FESDModelv1 for each Body Part 38
6-4 Confusion matrix of FESDModelv1 for each Joint 39
6-5 Confusion matrix of FESDModelv1 for each Body Half 40
6-6 Confusion Matrices of FESDModelv2 41
6-7 ROC Curves of FESDModelv2 42
6-8 Confusion matrix of FESDModelv2 for each Joint 43
6-9 Confusion matrix of FESDModelv2 for each Body Half 44

A-1 Number of Joints with error 53
A-2 Number of Joints with error per body half 54
A-3 Number of Joints with error per body part 54

B-1 Error Distribution of the Full Body by difficulty 55
B-2 Error Distribution of the Half Body by difficulty 56
B-3 Error Distribution of the body parts by difficulty 57
B-4 Error Distribution for each error class by difficulty 58
B-5 Error Distribution for each error class by joint 59
B-6 Error Distribution of the joints by difficulty 59

C-1 Full Body model training results 61
C-2 Half Body model training results 62
C-4 Body Parts model training results 64
C-9 Detailed Training results for the Joint Problem Set 66
C-10 Full Body Confusion Matrix by Body Half and Difficulty 67
C-11 Half Body Confusion Matrix by Body Half and Difficulty 67
C-12 Body Part Model Confusion Matrix by Body Half 68
C-13 Joint Model Confusion Matrix by Joint 68

D-1 Full Body model training results 69
D-2 Half Body model training results 70
D-3 Half Body Confusion Matrix by Body Half 70
D-5 Limb model training results 72
D-6 Body Parts Confusion Matrix by Body Part 73
D-11 Detailed Training results for the Joint Problem Set 75
D-12 Joint Model Confusion Matrix by Joint 76

List of Tables

3.1 The Confusion Matrix 7

4.1 Trivial Exercises 15
4.2 Easy Exercises 15
4.3 Medium Exercises 17
4.4 Difficult Exercises 17
4.5 The two possible errors for the skeleton 21
4.6 The four possible errors for the individual Joints. 21

5.1 Top 5 models for Accuracy and Performance 31

6.1 Test Results of FESDModelv1 35
6.2 Test Results of FESDModelv2 40

Chapter 1

Introduction

Human pose estimation (HPE), or skeleton detection, aims at detecting the pose or skeleton of a person based on visual information only. It finds many applications, from games to medical applications[1, 2, 3].

Gaming and entertainment are one of the most common applications of HPE. Games can use HPE in a way that makes the interaction between humans and computers very natural. One of the systems that kickstarted the use of depth cameras in games was the Xbox Kinect by Microsoft, which uses a depth camera, the Microsoft Kinect, to track the movement of the player and used this information to control the games.

Autonomous driving has been in development ever since humans replaced horses with cars[4]. However, the development of autonomous driving has been very slow. The main reason for this is that autonomous driving requires a lot of information about the environment. This information is usually provided by sensors that are installed in the car. However, sensors alone do not always suffice. In some cases, cars need to be able to estimate the pose of a human to make a decision. The posture of a human can be used to determine the action and therefore the future trajectory of the person.

To exactly emulate human movements in *Animation*, animators can either manually move the joints of a digital skeleton or they can use real human[1] actors to provide the movement for them. The manual creation of realistic movement is oftentimes very time-consuming and also error-prone. Therefore, animators often use real human actors to provide the movement for them. This provides animators with a skeleton and movement which is accurate and does not include human error.

To aid in the *Rehabilitation* of patients as well as to improve the quality of life of elderly people, HPE can be used to detect the pose of a person and provide feedback on the pose of the person during exercises[2].

Additionally, HPE can be used as a *Diagnostic tool* for all ages. For example, to detect Cerebral palsy (CP) usually, an MRI is used using human observations. However, MRIs are expensive and the expert knowledge to detect CP requires long training. HPE offers a low-cost alternative for the detection of CP risk using automatic movement assessment with comparable performance to standardised CP risk measureers[5].

Throughout all these applications HPE is a critical component that is required to be accurate. However, HPE is a difficult task that is prone to errors[6], which can be caused by different factors, such as the environment, the camera, and the person. These errors can cause the joints of the pose to be in the incorrect position or missing. This can cause

[1] Or animal

the pose estimation to be incorrect, and therefore, the human-computer interaction will be hampered. The goal of this thesis is to develop a preliminary method that allows for the detection of these errors such that the pose information can either be improved on them or handled accordingly.

One of the limiting factors for HPE is the user itself. If the posture is not as the model expects then errors might occur. This is especially true for applications that are designed for rehabilitation and exercise purposes. In these applications, the user is often elderly and has limited mobility, as is the case for games developed by SilverFit[2]. SilverFit is a serious gaming company that develops games for rehabilitation with a special focus on geriatric patients. In their games, SilverFit uses HPE to detect the pose of the player and use it to control the game to make exercise more enjoyable while promoting activity. This thesis is written in collaboration with SilverFit and aims at improving HPE by giving feedback on the errors in their games.

For some exercises designed by SilverFit and other companies, HPE is not sufficiently reliable to create an enjoyable experience for patients in every environment. Especially sedentary exercises often cause the HPE to fail or to produce unreliable results.

To understand the errors that can occur during HPE I pose three research questions. (A) What errors occur during HPE and how can these errors be reproduced in a controlled manner? (B) How can a dataset of multiple modalities be captured, to analyse if the previous observations about problems during pose estimation are correct? (C) How can the previously captured and labelled dataset be used to train a model using multi-modal data to determine if a joint is faulty or not?

To answer the questions posed, first, the most common error sources are analysed. During the analysis of the problems, different factors are discussed which might influence the human pose estimation. Based on these factors exercises are designed to emulate different scenarios with different difficulties. This is discussed in section 4.1.

Then a custom tool, FESDData, was developed which allows for the capture and labelling of multi-modal data, including RGB, Depth and Pose data, as well as recording metadata such as the exercise name and the time stamps. The tool allows capturing predefined exercises and labelling each joint of each captured frame with error labels. The data collection and processing are discussed in section 4.2. The collected data forms the dataset, FESDDataset.

Using FESDDataset a data loader and model are derived. The data loader performs the necessary preprocessing steps, such as data augmentation, data balancing and resizing of the modalities. Then the models, FESDModelv1 and FESDModelv2, are trained to detect faulty joints. Additionally, each of the two proposed models are developed with different problem sets in mind. This is discussed in section 5. Finally, the preliminary experiments are evaluated and the results are discussed in section 6.

[2] https://www.silverfit.com/en/

Chapter 2

Related Work

Human Pose Estimation To detect errors in HPE the methods of capturing the human pose from different modalities are essential. Multiple different human pose estimators have been developed using different modalities and focussing on different parts of the body. For example, OpenPose has developed a general human pose estimator[7], a hand pose estimator[8] and an estimator that is capable of detecting multiple people[9]. Z. Cao et al. achieve this by using solely RGB data.

A method that uses RGB data in combination with errors for estimating the correct pose, is proposed by Joao Carreira et al.[10]. In their paper, the authors extract the features of both input and output spaces. This enables Joao Carreira et al. to develop a self-correcting model using Iterative Error Feedback.

Other methods use point clouds which are extracted from depth data. Point clouds are a representation of depth data which represents the environment using points. is commonly used in autonomous driving to represent the real world more accurately and to describe complex objects in the environment. However, conventional feature extraction using CNNs proves difficult to apply since most point clouds are not ordered and not dense so locality cannot be ensured. PointCNN, proposed by Yangyan Li et al.[11], combats this problem by learning an $\mathcal{X}$-Transformation to then extract the features using a generalised CNN.

Datasets There are different datasets encompassing different environments and modalities. The KITTI dataset is captured using LIDaR cameras and contains both depth and RGB data[12]. One of the largest datasets specifically for HPE and its applications is Human3.6M[13]. Human3.6M is a large-scale dataset containing RGB, Depth and Pose information.

Action Recognition One of the uses of HPE is action recognition. Action recognition is the extraction of pre-defined actions from different modalities.

To use different modalities in combination Seddik et al. compare different fusion methods for action recognition[14]. After detecting the features for each of the modalities, RGB data, Depth data and Pose data, they fuse the features using different methods.

Chapter 3

Fundamentals

For a better understanding of error detection in HPE fundamentals are discussed in this section.

3.1 Human pose estimation

There is a wide variety of how humans can interact with computers. Ranging from early punch cards to touch screens, the methods have evolved to be more natural and intuitive. In recent years, the use of cameras has become more popular, since they require no physical contact with a computer and therefore allow users to seamlessly interact with an application.

Pose visualisation Different methods to estimate the pose of a human have been developed, such as OpenPose, or Nuitrack. Depending on the usage of the pose estimation, different methods are used to visualise the pose of a human. These visualisations may provide different information about the pose of a human.

There are mainly three different ways the human pose can be visualised. The first and most basic way is to visualise the pose as a kinematic representation, in which a "skeleton" with bones and joints is used to represent the pose of a human. The skeleton is made up of joints, which are connected by bones. The number of joints and bones can vary, for example, the representation shown in figure 3-1(a) uses 15 joints and 14 bones. The representation of a joint in the data varies, but it is usually a 2D point on the image plane or 3D point in space for example in a point cloud. In some cases, the joint representation is provided with a keypoint orientation that enables the clear representation of all degrees of freedoms joints have[15]. Additionally, in some cases, especially if the human pose was estimated using a neural network, a confidence rating or score is added which can be used to determine the reliability of the joint.

The second way to visualise a human pose is by using a 2D silhouette or 2D rectangles and shapes. These methods are also called contour-based methods. An example of contour-based methods was introduced by Yunheng Liu[16]. Contour-based methods are often used in combination with a skeleton representation. The skeleton is used to determine the location of the joints, while the contour is used to determine the shape of the body. The silhouette representation is visualised in figure 3-1(b).

Finally, the third way to represent a human pose is with a three-dimensional volume this is shown in figure 3-1(c). This volume may be simple cylindrical shapes or a body

mesh. A body mesh is a 3D representation of the body, which is made up of vertices and triangles.

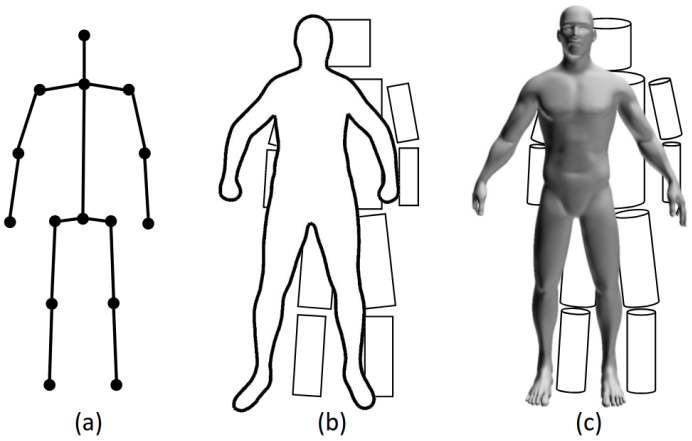

Figure 3-1: Different representations of the human pose. (a) Kinematic representation. (b) Contour representation. (c) 3D volume representation. [17]

Data sources The data that is acquired influences the way the human pose can be estimated. The most common data source is RGB images or videos. RGB videos are any videos that are captured with normal cameras that record the colour of the scene. The provided data can be either from a video or a stream of data or a still image. There is a large number of datasets that can be used to train and test poses estimation algorithms from RGB data. Some of the most common datasets are the MPII Human Pose Dataset[18], the COCO dataset[19], and HumanEva-I dataset[20].

Additionally, some datasets are captured with depth cameras. Depth cameras are cameras that can record, in addition to the colour channels, the depth of the scene. Different methods to acquire depth data have been developed. The most commonly used depth cameras emit an infrared light pattern to measure the depth of a scene. This depth information can be used to improve the accuracy of the pose estimation. Some of the most common datasets that are captured with depth cameras are the MRI dataset[21], and the Human3.6M dataset[13].

Finally, there are also methods of HPE that use point clouds. Point clouds are a collection of points in space, which can be used to represent the shape of an object. Each point in the point cloud represents a point in the environment. The point cloud is created using the depth information of a scene and the intrinsics of a camera, i.e. the field of view and the focal point of the camera. A point cloud is a reconstruction of the real-world scene. Point clouds are often used in combination with RGB data. Some of the most common datasets that are captured with depth cameras are the SMMC-10 dataset[22], and the EVAL dataset[23]. However, any RGB and depth dataset can be used to train and test point cloud-based pose estimation algorithms if the camera intrinsics and extrinsic, such as the horizontal and vertical field of view, the focal point, and the depth units are known. With the knowledge of these parameters, the depth information can be converted to a point cloud and if the RGB data is in line with the depth data, the individual points can be coloured accordingly.

3.2 Convolutional Neural Networks

Convolutional neural networks(CNN) are a type of feed-forward neural network that are commonly used for computer vision tasks. As the name suggests, CNN apply convolutional operations in some of the layers of the network architechture. A convulutional operation is an integral over two functions to determine the amount of overlap of these functions, resulting in a third function. In CNN, the first function is usually an image or rather a matrix representation of an image and the second function is a matrix, that is changed throughout the course of network training. This operation then results in a new matrix. This is used to extract local features from an image.

In most cases, the features that are produced by multiple convolutional layers are forwarded into fully connected layers. These layers learn the features based on the input data. In case of image classification tasks, the fully connected layers are usually followed by a softmax layer to calculate the probability of each class. The class with the highest probability is then used as the prediction of the network for the given input.

Since convolutional neural networks require a lot of data to be trained properly, transfer learning is applied in some cases. Transfer learning is a technique that uses a pre-trained model to extract features from the input data. The pre-trained model is usually trained on a large dataset, such as ImageNet[24]. The pre-trained model is then used to extract features from the input data. These features are then used to train a new model. This allows the new model to be trained with less data and therefore less time. Additionally, the pre-trained model is usually trained on a large dataset and therefore the features that are extracted are more general and can be used for different tasks.

3.3 Evaluation metrics

To rightfully evaluate the performance and accuracy of a model, different metrics are used. In this section, some metrics that can be used to evaluate the performance of a model are discussed.

3.3.1 Confusion Matrix

A confusion matrix is a graph which represents the false positives and the true negatives in a single graph. The confusion matrix can be seen in table 3.1. The confusion matrix is useful to visualise the performance of a model.

Table 3.1: The confusion matrix as a metric for binary classification. The results of the prediction (PRED), left, and the actual ground truth (GT), top.

PRED \GT	TRUE	FALSE
TRUE	TP	FP
FALSE	FN	TN

3.3.2 Percentage of positive Guesses

The percentage of positive guesses is an indicator of the performance of a model. For example, if the dataset is unbalanced, the accuracy might be sufficiently good when only

guessing for the majority class. In those cases, the percentage of positive guesses would either be 0% or 100%. Therefore, the percentage of positive guesses is used to determine if the model is biased toward a specific class. The equation for the percentage of positive guesses can be seen in equation 3.1. In this thesis, the percentage of positive guesses is sometimes referred to as $\frac{p}{p+n}$ as it is the ratio of the number of positive guesses p to the total number of guesses $p+n$.

$$\text{Percentage of positive guesses} = \frac{\text{Number of positive guesses}}{\text{Number of guesses}} = \frac{tp+fp}{tp+fp+tn+fn} \tag{3.1}$$

3.3.3 Receiver Operating Characteristic Curve

The receiver operating characteristic curve (ROC curve) is a metric that shows the performance of a model performing binary classification tasks. It plots the true positive rate $\frac{TP}{TP+FN}$ against the false positive rate $\frac{FP}{FP+TN}$. This allows for the evaluation of a classifier without the influence of class distribution. An interpretation of the ROC Curve can be seen in figure 3-2

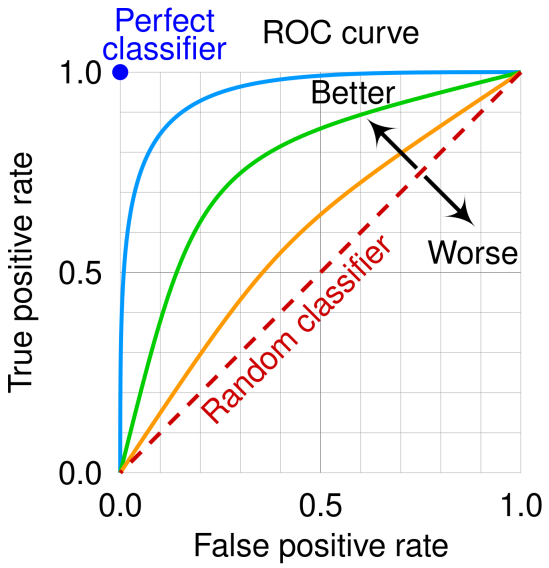

Figure 3-2: An interpretation of the ROC curve. The plotted lines are examples of exceedingly good classifiers, with orange being the worst and blue being the best.[25]

3.3.4 Accuracy, Precision, Recall and F1-Score

The accuracy of a prediction is the ratio of the number of correct predictions to the total number of predictions. The accuracy is calculated using equation 3.2. The accuracy is a good indicator of the performance of a model if the dataset is balanced. However, if the dataset is unbalanced, the accuracy might be sufficiently good when only guessing for the majority class.

$$\text{Accuracy} = \frac{\text{Number of correct predictions}}{\text{Number of predictions}} = \frac{tp+tn}{tp+fp+tn+fn} \tag{3.2}$$

The precision of a prediction is the ratio of the number of correct positive predictions to the total number of positive predictions. The precision is calculated using equation 3.3.

$$\text{Precision} = \frac{\text{Number of correct positive predictions}}{\text{Number of positive predictions}} = \frac{tp}{tp + fp} \tag{3.3}$$

The recall of a prediction is the ratio of the number of correct positive predictions to the total number of positive samples. The recall is calculated using equation 3.4.

$$\text{Recall} = \frac{\text{Number of correct positive predictions}}{\text{Number of positive samples}} = \frac{tp}{tp + fn} \tag{3.4}$$

Finally, the F1-Score is the harmonic mean of the precision and the recall. The F1-Score is calculated using equation 3.5. The F1-Score is a good indicator of the performance of a model if the dataset is unbalanced since it takes both the precision and the recall into account.

$$\text{F1-Score} = 2 \cdot \frac{\text{Precision} \cdot \text{Recall}}{\text{Precision} + \text{Recall}} = \frac{2 \cdot tp}{2 \cdot tp + fp + fn} \tag{3.5}$$

3.3.5 Cohen's kappa coefficient

Cohen's kappa coefficient is an inter-rater reliability measure[26]. This means that two different raters are compared. In the case of a binary classification, the formula for Cohen's Kappa can be seen in equation 3.6. In the case of prediction, the two raters are the ground truth and the prediction.

$$\kappa = \frac{2(tp \cdot tn - fn \cdot fp)}{(tp + fp)(fp + tn) + (tp + fn)(fn + tn)} \tag{3.6}$$

If Cohens Kappa is less than 0, there is no agreement between the two raters. If the kappa score is less than 0.5 there is a slight agreement. A score of more than 0.8 is considered almost perfect. However, the "exact" values vary from application to application.

Chapter 4

FESDData - Data Acquisition and Labelling of FESDDataset

One of the most important aspects of machine learning is data acquisition since a machine learning algorithm can only be as good as the data provided. In this thesis, a custom tool is developed which is capable of capturing and labelling multi-modal data. The tool is called **F**ault **E**stimator for **S**keleton **D**etection **Data** processor (FESDData). It is capable of capturing RGB-D data (RGB and the corresponding depth) from multiple different RGB-D cameras as well as pose data calculated by Nuitrack, which was developed by 3DiVi Inc[1]. Nuitrack was chosen as the pose estimation backbone since it provided the support of multiple different camera models as well as the ability to extract the RGB-D data and pose data simultaneously.

In addition to Nuitrack, FESDData is capable of calculating the pose information using OpenPose after the recording is done. This offers future support for other pose estimation backbones. However, OpenPose is not used in the scope of this thesis.

FESDData is designed to be easily used by anyone and to require minimal setup or tweaking. It allows for the rapid capture of RGB-D datasets with the pre-labelling of multiple different exercises. The parameters can be adapted to capture datasets for many different applications, e.g. action detection, where HPE is used to identify an action.

For this research, exercises have been derived which are designed to emulate different scenarios with different difficulties. These exercises are discussed in section 4.1. The labelling of errors in the data requires domain-specific knowledge and is therefore done manually. The resulting dataset, FESDDataset, is discussed in section 4.7. It consists of the RGB-D data as well as the pose data and the labels for the errors for each of the joints in the pose.

In this chapter, the approach to the design of the exercises is discussed by showing the difficulties of HPE. Furthermore, the data acquisition and labelling process is discussed. Finally, the features of the dataset are presented.

4.1 Challenges in HPE

In this chapter, possible faults and difficulties that occur during HPE are discussed. These difficulties are caused by different factors, such as the environment, the camera, the person, and the software.

[1] https://nuitrack.com/

These difficulties are important to understand, as they can cause the joints to be in the incorrect position or missing. Leading to an incorrect estimation of the pose estimation, and therefore, the human-computer interaction will be hampered.

4.1.1 Environment

The environment in which the data is recorded is crucial to the quality of the pose estimation. The mentioned difficulties depend on how the method itself works. For example, if a method uses RGB data, the background might be an issue, whereas if a method uses depth data, the lighting is more of an issue.

Background

The background of the scene can cause difficulties in the HPE process. Methods using RGB cameras might have difficulties detecting the difference between the foreground and the background. In RGB-D-based methods, the background can cause depth ambiguities which might even prevent the human from being detectable, especially if the background is reflective, or too close to the user.

Lighting

While RBG cameras are to some extent insensitive to the amount of incoming light, RGB-D cameras are highly influenced by the lighting. Most RGB-D cameras use infrared light to determine the depth of the scene, some use a pattern of infrared light that is projected onto the scene to be distorted by physical objects, and some use the time-of-flight method to determine the depth of the scene. The issue that arises with infrared light is that it is also emitted by the sun. This means that light emitted by the sun can interfere with the detection of the infrared light emitted by the camera. This can cause the depth of the scene to be inaccurate or missing in parts with a high intensity of sunlight.

To reduce the effect of the sunlight, the camera can be placed in a room with curtains or blinds. This will reduce the amount of sunlight that enters the room and therefore reduce the effect of the sunlight on the camera. Since lighting is hard to perfectly reproduce without a controlled environment, the lighting is not varied throughout the experiments. Therefore, all of the experiments were conducted in a room without any natural light or during the night.

However, if a method heavily relies on RGB data for the pose estimation, eliminating any form of light is not a valid option since then the data that can be gathered by RGB cameras in low light environments is limited and may result in a wrong pose.

Objects

The objects in the scene may cause issues in the HPE process if they either occlude or are too close to the user. Occlusion can cause inaccurate or missing joints. Whereas objects that are too close to the user can cause joints to move to these objects instead.

Chair

If the exercise is performed in a sitting position the chair might influence the accuracy of HPE. For example, wheelchairs pose a problem in some estimators, but a significant part of

users who use pose estimation for rehabilitation games are using wheelchairs due to health conditions. Furthermore, bulky chairs that go higher than the head may prevent accurate head detection and therefore, negatively impact the pose estimation, since in some pose estimators the head is used as an ankor point as it is usually reliable.

4.1.2 Camera

The two main difficulties that can occur with the camera setup are the camera position and the camera angle. Additionally, the camera itself can make the pose estimation process more difficult.

Distance to the camera

The distance of the camera to the user affects the quality of the pose estimation in multiple ways. Firstly, if the user is too close to the camera, the camera might not have the complete body in the frame. The legs and arms might be off the frame preventing them to be estimated properly. Additionally, depth cameras can only detect the depth for a specific range, so if a user is too close they might not be visible to the depth camera.

However, if the user is too far away from the camera, the person might be too small to be detected reliably. Additionally, depth cameras operate at different depth ranges. If a user is too far away from the camera it will not be visible to the depth camera. This range varies from camera to camera and depends on the method of detection.

Camera Angle

When considering angles the main focus lies on pitch and roll. For the experiments, the yaw is assumed as fixed and directed facing the user, such that the user is in the centre. The camera is set up such that there is no or minimal roll as all applications ensure that the camera is not tilted to the side.

The pitch may introduce or reduce the occlusion of joints by other joints. It also influences which area is best for HPE. The pitch of a camera depends on what the main application is. For example, if the legs are not considered then the pitch could be used to focus more on the upper body.

Camera Resolution

The resolution of the camera, or rather the resolution of the image captured by the camera influences the information that can be gathered about the human and therefore influence the performance of the pose estimation. Also here the application and specific range are important for choosing the right resolution. If a user is far away a higher resolution is needed to detect the pose reliably.

4.1.3 Person

Finally, one of the main error sources of HPE is the person. The person can cause difficulties in the HPE process by moving, wearing specific clothes, or having a different body posture. Body posture is of special importance for SilverFit since the company specialises in games for rehabilitation and elderly people. Elderly people have different body postures than the average person, which can cause difficulties in the HPE process.

Clothes

As mentioned earlier, most RGB-D cameras use infrared light to determine the depth of the scene. This means that the clothes of the user can cause more or less absorption of light and therefore influence the detected depth. This can cause the joints to be detected in the wrong position or not at all. This is especially the case for dark clothes, as they absorb more light than light clothes.

Furthermore, bulky clothes or skirts and dresses may influence the pose, since the exact position of the legs is not visible.

Training Equipment

To make exercises more challenging some physiotherapists use additional training equipment. This could be weights that are held in the hand or weights that are attached to the ankles. These weights change the outline of the body and therefore influence the pose estimation.

Exercises

Finally, the most important factor is the exercise that is carried out. In this section, both exercises that are easy to detect as well as some exercises that are difficult to detect are proposed.

These exercises might not be the most realistic, but they represent common issues with pose estimation in a reproducible manner. Furthermore, these exercises are not too difficult to perform, which makes them suitable for testing the pose estimators. The difficulty rating of the exercise might not reflect the difficulty of the exercise for the user, but it does reflect the difficulty of the exercise for the pose estimator.

The exercises are numbered according to the difficulty. An example of the naming of the exercises can be seen here:

$$\underbrace{E}_{\text{Exercise}} - \overbrace{2}^{\text{Difficulty}} . \underbrace{02}_{\text{Exercise Id}}$$

The different difficulties are (0) Trivial, (1) Easy, (2) Medium, and (3) Hard. The Exercise Id is the numbering of the exercises, not necessarily in order of difficulty.

Trivial Exercises Trivial exercises are exercises that are easy to detect and are therefore good for testing the pose estimators. The exercises do not involve any movement, which makes detecting the joints easier. The two trivial exercises can be seen in table 4.1. Example images of the exercises can be seen in figure 4-1.

Easy Exercises Easy exercises are essential for creating a good baseline of how the pose estimators should work. The exercises include no self-occlusion and are recorded in a standing position, which is generally the easiest position to detect. The easy exercises can be seen in table 4.2. Example images of the exercises can be seen in figure 4-2.

Medium Exercises Exercises which are performed in a seated position are harder to detect since parts of the body are occluded. Medium exercises focus on exercises, which are

Table 4.1: The two Trivial Exercises, E-0.00 and E-0.01.

Exercise	Short Description	Challenge
E-0.00	Arms hanging to the side	This exercise is very easy since no part of the body is occluded by any other part. Additionally, the joints are not moving.
E-0.01	Arms extended to the side	The arms are no longer in a natural position but still not occluded and no joint is moving

(a) E-0.00 (b) E-0.01

Figure 4-1: The two trivial exercises. (4-1a) Arms hanging to the side. (4-1b) Arms extended to the side.

performed in a seated position. The medium exercises can be seen in table 4.3. Example images of the exercises can be seen in figure 4-3.

Difficult Exercises Difficult exercises are exercises that are performed in a standing position and involve leg movement. Leg joints are harder to detect than arm joints and therefore pose a greater challenge for pose estimators. These exercises will be in a seating position and with a difficult posture, such as leaning forward. The difference in posture aims at creating a realistic representation of real-world exercises.

Tölgyessy et al. found that facing away from the camera decreases the accuracy of HPE

Table 4.2: The Easy exercises, E-1.00 through E-1.03. The easy exercises include both standing and sitting exercises.

Exercise	Short Description	Challenge
E-1.00	Raising the arms to the side	Now the arms are no longer stationary. Still, there is no occlusion.
E-1.01	Raising the arms to the front	The arms occlude themselves and part of the body.
E-1.02	Raise the knees to the chest	The legs now occlude parts of the hip.
E-1.03	Sit in a chair motionless	Sitting positions are more challenging to detect than standing positions since there is now a chair in the background and the body occludes itself.

(a) E-1.00 (b) E-1.00 (c) E-1.01

(d) E-1.01 (e) E-1.02 (f) E-1.03

Figure 4-2: The four easy exercises. (4-2a, 4-2b) Raising the arms to the side. (4-2c, 4-2d) Raising the arms to the front. (4-2e) Raising the knee to the chest. (4-2f) Sitting in a chair motionless.

due to self-occlusion. [6] Therefore, some of the exercises will be performed facing away from the camera. The difficult exercises can be seen in table 4.4. Example images of the exercises can be seen in figure 4-4.

Table 4.3: The Medium exercises, E-2.00 through E-2.03. The medium exercises are all in a sitting position.

Exercise	**Short Description**	**Challenge**
E-2.00	Raising the arms to the side while sitting	Now the arms are no longer stationary. With added difficulty since the user is now sitting.
E-2.01	Raising the arms to the front while sitting	The arms might occlude themselves and part of the body. Additionally, the person is now sitting down
E-2.02	Crossing the arms in front of the chest while sitting	The arms now occlude large parts of the upper body.
E-2.03	Raising the knee to the chest while sitting	More parts of the upper body are occluded and not seen by the camera.

Table 4.4: The Difficult exercises, E-3.00 through E-3.02. The difficult exercises are all in a standing position.

Exercise	**Short Description**	**Challenge**
E-3.00	Bowing toward the camera	The head is often used as an anchor point for the skeleton as it is quite stable. When bowing forward the head is no longer easily detectable.
E-3.01	Raising the knee leaning forward	Leaning forward increases the difficulty since the position is not natural
E-2.02	Raising the knee leaning forward while sitting and facing away from the camera	Facing away from the camera makes it more difficult to detect the pose and induces more occlusion.

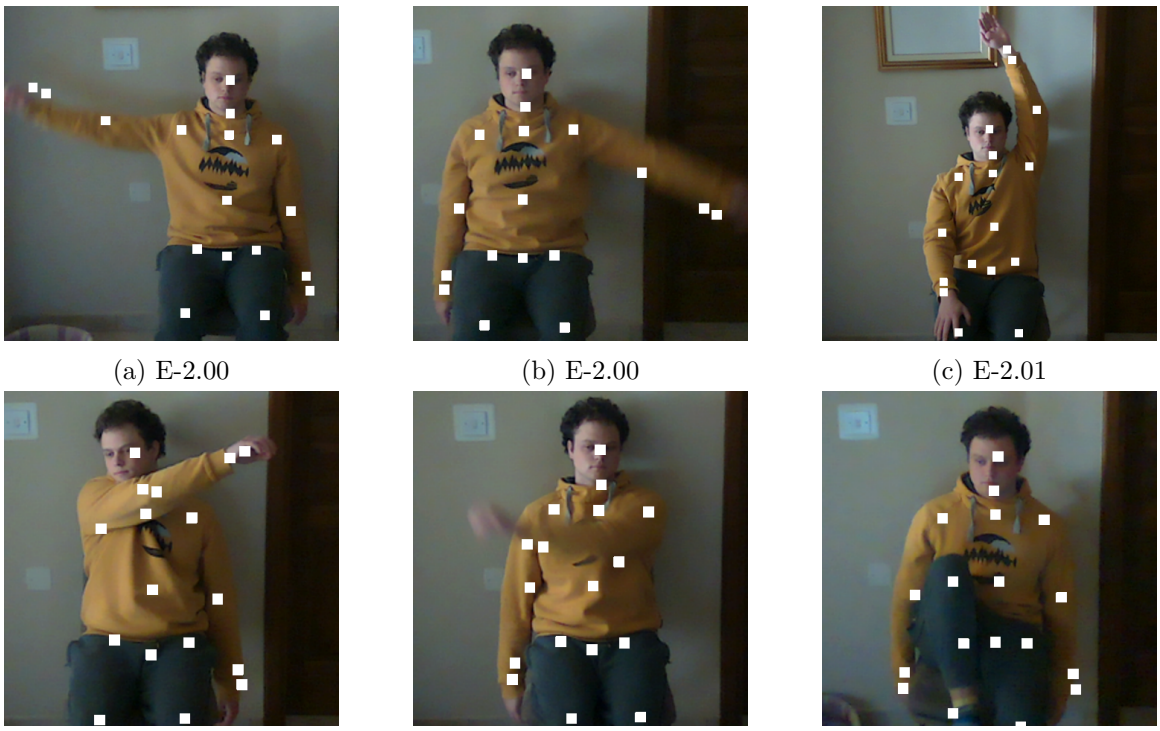

(a) E-2.00 (b) E-2.00 (c) E-2.01

(d) E-2.02 (e) E-2.02 (f) E-2.03

Figure 4-3: The four medium exercises. (4-3a, 4-3b) Raising the arms to the side while sitting. (4-3c) Raising the arms to the front while sitting. (4-3d, 4-3e) Crossing the arms in front of the chest while sitting. (4-3f) Raising the knee up to the chest while sitting.

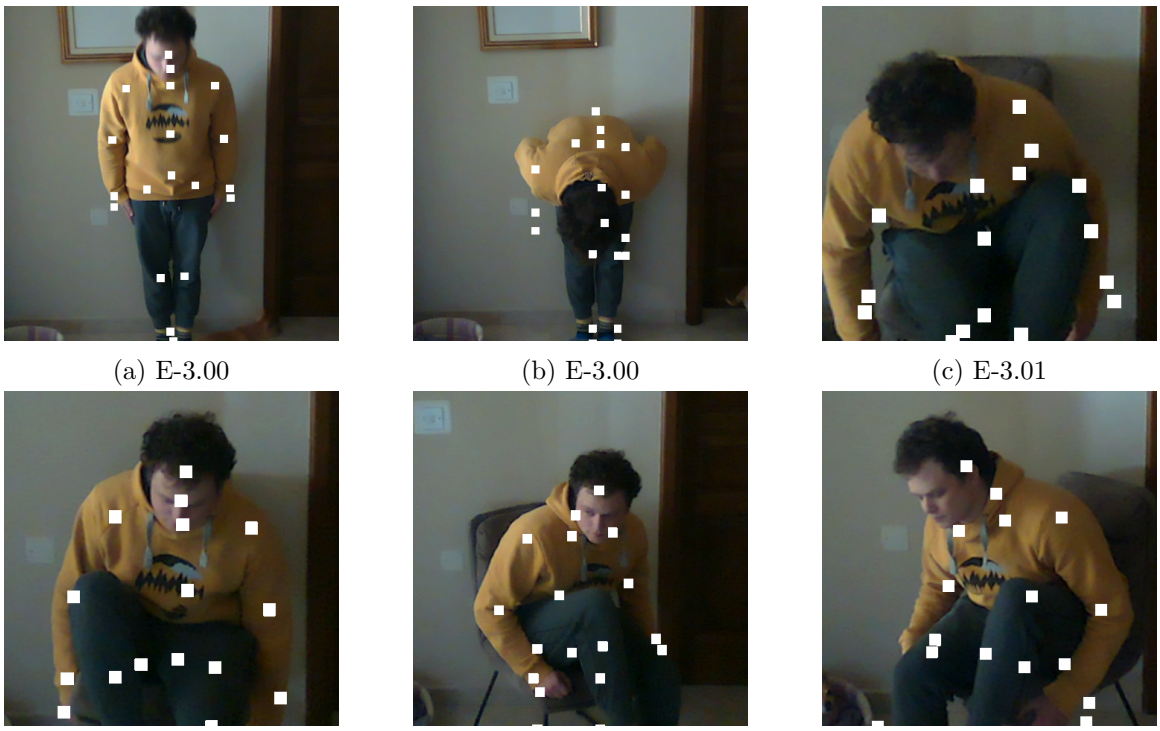

(a) E-3.00 (b) E-3.00 (c) E-3.01

(d) E-3.01 (e) E-3.02 (f) E-3.02

Figure 4-4: The three difficult exercises. (4-4a 4-4b) Bowing toward the camera. (4-4c, 4-4d) Raising the knee leaning forward. (4-4e, 4-4f) Raising the knee leaning forward while sitting and facing away from the camera. Some of the exercises contain errors in the sample.

4.2 Data acquisition

Different modalities were captured to create a dataset that reproduces a real-world application of HPE for RGB-D cameras, i.e. cameras that capture RGB and depth. The different modalities are RGB data, depth data, and joint data. While the Nuitrack SDK offers to capture the data from the RGB-D cameras and the joint data, the recorded files cannot, at the time of writing, be read without using the Nuitrack SDK. Therefore, FESDData, a custom RGB-D+HPE capturing and labelling tool was developed.

FESDData has two main uses. Firstly, it allows capturing predefined, as well as custom, exercises repeatedly automatically making the capturing experience when capturing many different exercises with multiple repetitions more comfortable. Secondly, it allows reviewing and labelling the captured data with error labels. The lightweight nature of FESDData allows it to seamlessly capture both the RGB-D stream and the skeleton data at the same time while ensuring a stable fast framerate. The dataset that is used by FESDModel was captured at a framerate of 30 frames per second. The interface of FESDData can be seen in figure 4-5. On the left side of the image the interface can be seen and on the right, there is an example for data labelling of Exercise E1-02.

4.3 Data layout

As mentioned earlier, the dataset is made up of multiple different modalities. There are two separate visual streams, the RGB stream, and the depth stream, as well as the estimated human pose, the relative time stamps of each frame, and the recording metadata. The recording metadata includes information about the camera, such as the horizontal as well as the vertical field of view, and the exercise. The exercise is captured as an Id and a separate file exists containing all exercises with a description.

The visual streams are normalised and combined into a single file. OpenCV is used to store the RGB and the depth data into a single matrix and after the stream into a single file per frame. The RGB data is normalised to have values between 0 and 1, whereas the depth data is stored in meters.

The pose that is estimated by Nuitrack, as well as the error labels, are stored in a separate JSON file. The separate frames are stored in a list of frames. Each frame contains a list of all people that were detected. Each person contains a list of joints as well as an error label, and an Id. Each joint is stored with real-world 3D coordinates which are stored in meters. These real-world coordinates are labelled x, y, and z. Additionally, the 2D

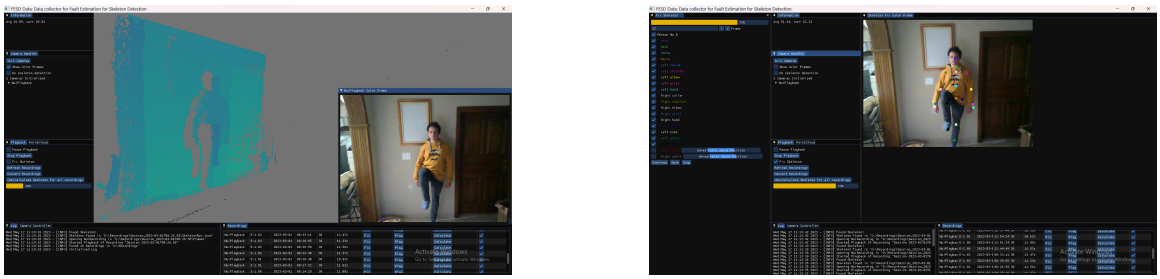

Figure 4-5: A screenshot of the user interface with its two main components. On the left side, the user interface during streaming and recording can be seen and on the right side an example of data labelling.

projection on the image plain and depth of the joint are stored in image coordinates and meters for the depth. The 2D projection is labelled u and v and the depth is labelled d.

The error label is an integer which is the error id specific for joint and skeleton errors. The errors corresponding to the error ids are explained in section 4.4.

4.4 Data labeling

A large part of the data preparation is the labelling of the data. The data is labelled with error labels. There are two different layers which can be labelled as erroneous. First, there are skeleton errors that occur when the pose estimator detects a human in places where there are no humans. Second, there are joint errors that occur when the pose estimator detects a joint in the wrong place.

For example, the estimator might label the left foot as the right foot. This is a common error, especially when the body parts are close to each other. An estimator might also not detect a joint at all. This might be caused by occlusion, be it by another joint, an object, or by the image border. Most applications avoid the last cause for occlusion by defining a minimum distance from the camera and specific camera placement to ensure that the user is always fully in view.

The possible error labels for the skeleton itself can be seen in table 4.5. Table 4.6, shows the different error labels for the individual joints of the skeleton.

Table 4.5: The two possible errors for the skeleton

Label	**Error Name**	**Example**
0	No Error	The skeleton is exactly aligned to the body
1	Error	The skeleton is in a different location and not on a body

Table 4.6: The four possible errors for the individual Joints.

Label	**Error Name**	**Example**
0	No Error	The joint is exactly aligned to the position where it is supposed to be
1	Missing Joint	The joint is not detected at all
2	Wrong Joint Position	The joint is somewhere outside the body
3	Different Joint Position	The joint for the left foot is in the position of the right foot

Implicitly, the errors shown in table 4.6 create two simpler general labels. Either a joint is faulty, i.e. the error label is 1, 2, or 3, or it is not faulty, i.e. the error label is 0.

4.5 Problem Sets

To create different abstraction levels problem sets are defined. The problem sets are defined by the number of objects that are considered and are defined as erroneous. There are four different problem sets. The first problem set is the *Joint* problem set. In this problem set,

each joint is considered as a single object. The second problem set, the *Body Part* problem set, is to consider each body part, i.e. the individual arms, legs, torso, and head. The third problem set is the *Half Body* problem set. In this problem set the upper and the lower body are the areas that are considered. Finally, only the whole body is considered in the *Full Body* problem set.

To determine the threshold at which each area is considered faulty, the distribution of joints with errors was calculated for each of the areas. Using this distribution the threshold was picked at the 50th percentile. It was found that when considering the full body as an area, the body is considered faulty if more than two joints in the pose are faulty. When considering the lower and upper body, one or more and more than two faulty joints are needed for the area to be considered faulty. For the body parts to be considered faulty one joint within the specific part needs to be faulty, except for the right and left leg, where two joints need to be faulty.

The different problem sets are visualised in Figure 4-6.

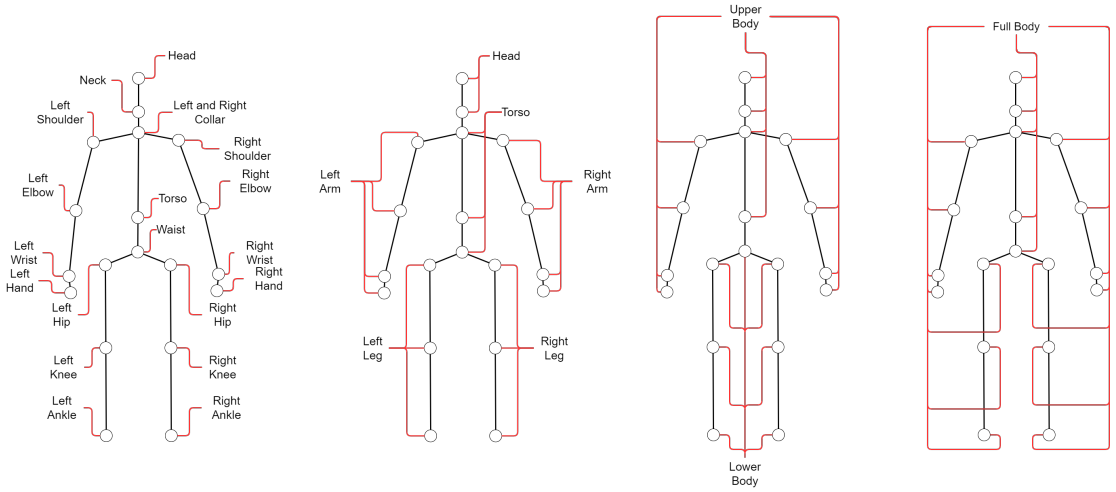

(a) Joint Problem Set

(b) Body Part Problem Set

(c) Half Body Problem Set

(d) Full Body Problem Set

Figure 4-6: The visualisation of the different problem sets, (a) Joint Problem Set, (b) Body Part Problem Set, (c) Half Body Problem Set, and (d) Full Bod Problem Set.

4.6 Recording Setup

Multiple iterations of the recording process were run to find the best possible setup, which reduces the light interference as much as possible and which offers the best results with the resources at hand. The camera setup that is used by SilverFit was reproduced. At SilverFit the camera is mounted at $175cm$ above the floor. The camera that is used has an accelerometer which was used to adjust the camera angle relative to the ground. The camera is angled downward at a $70°$ angle. To record the dataset an Intel Realsense L515 camera was used. Additionally, for the preliminary analysis of errors an Orbbec Astra+ and a Microsoft Kinect v2 were used.

4.7 Dataset Analysis

To get a better understanding of the data and how it can be used it has to be analysed. Especially the distribution of errors within the dataset is important to understand the balance of the dataset and to understand possible outcomes of the model development phase.

4.7.1 Distribution of Errors

An important aspect of the dataset is the structure and distribution of data and their labels. In total, all 13 exercises mentioned in section 4.1.3 were recorded twice. Each recording session consists of exactly 300 frames, resulting in a total of 7800 frames. Of these, every 10th frame was labelled for a total of 780 labelled frames, which were used for the preliminary model development.

When multiple persons are detected one person might be incorrectly detected in the background. While analysing the data the person that is not labelled as faulty is selected whenever possible. If a person is labelled as faulty each joint is marked as in an unrealistic position.

An important factor in how well a model can be trained on data is the balance of the dataset. In this case, the dataset is balanced by the error labels.

Full Body Error Distribution

In Figure 4-7 the error distribution of the Full body problem set can be seen. It can be observed that the distribution of errors is reasonably equal with a difference of 10%.

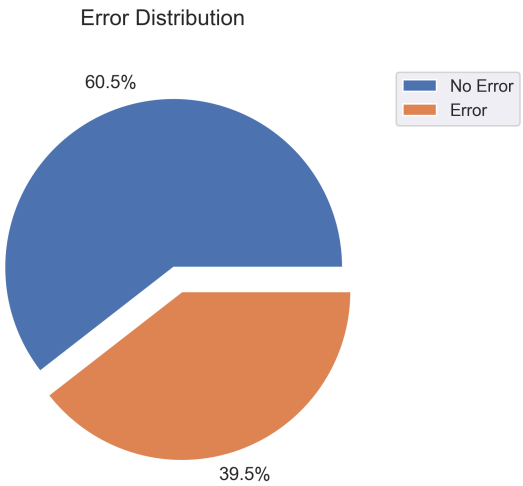

Figure 4-7: The distribution of Errors of the full body problem set.

Half Body Error Distribution

Figure 4-8 shows a discrepancy between the error distribution of the lower body (65.4% Errors) and the upper body (32.4% Errors). The upper body is generally more stable and less error-prone than the lower body.

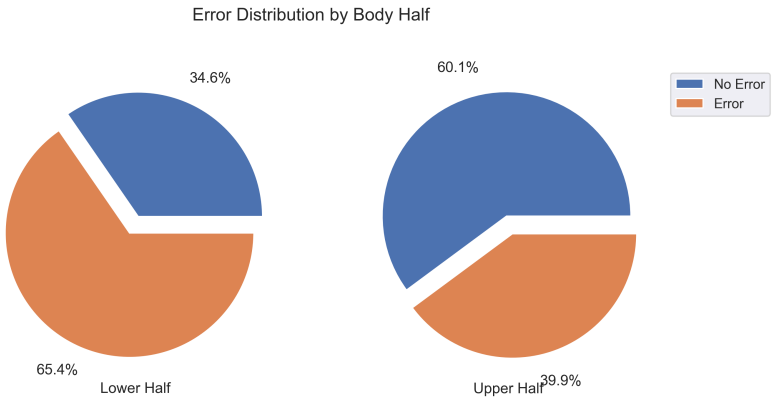

Figure 4-8: The distribution of Errors of the half body problem set.

Body part Error Distribution

The error distribution of each body part is shown in figure 4-9. It can be observed that the errors of the body parts are individually very unbalanced. The left arm is the most error-prone body part with 24.1% of the joints being faulty. The torso is the least error-prone body part with 10.3% of the joints being faulty.

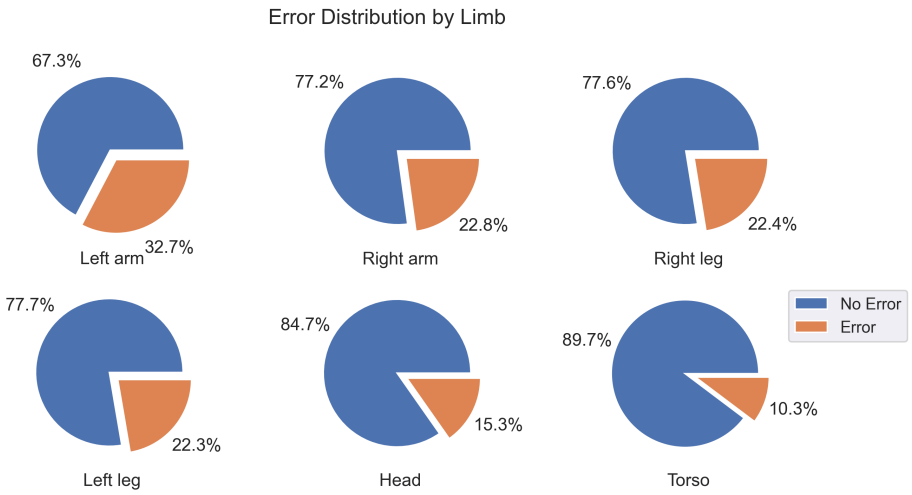

Figure 4-9: The distribution of errors of the body part problem set.

Joint Error Distribution

Figure 4-10 shows that the major part of the errors that occur are errors with the label 2, i.e. the joint is detected in the wrong place. The second most common error is label 1, i.e. the joint is not detected at all. The least common error is label 3, i.e. the joint is detected in the approximate position of where another joint should be.

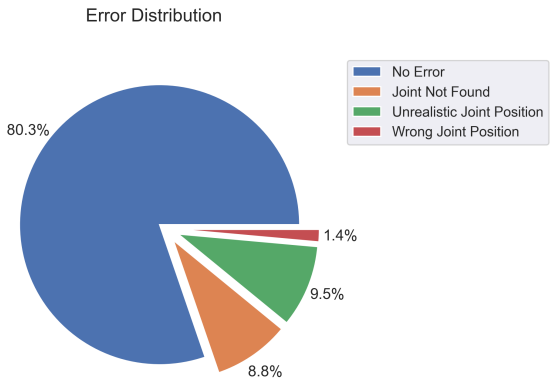

Figure 4-10: The distribution of each error class.

Chapter 5

FESDModel - Preliminary Experiments for Model development

While there could be multiple approaches to fault estimation, a deep-learning approach using deep convolutional neural networks(CNN) has been chosen. The reason for this is that CNNs have shown to be very successful in many different fields, especially in computer vision tasks, such as image classification, object detection, and image segmentation.

Other possible solutions could be to use rule-based systems, which use inverse kinematics, or use frame-to-frame joint comparison to detect discrepancies, however, these are quite limited and might result in either too many false positives or false negatives. Furthermore, these rules, such as the frame-to-frame joint comparison, are not always applicable to all types of movements, and therefore might not be able to detect all types of faults in all cases.

Here two different models are proposed as they could be designed for this kind of task on a dataset consisting of three different modalities, RGB, Depth, and Pose Data.

5.1 Model architecture

To approach the problem of error estimation, two different model architectures are devised. The first model architecture, FESDModelv1, is a deep convolutional neural network that uses the RGB, Depth, and Pose data as separate inputs. This model can be seen in figure 5-1.

The second model architecture, FESDModelv2, utilises transfer learning to extract the features of the input data using a pre-trained model. The architecture of FESDModelv2 can be seen in figure 5-2. Both models are trained to predict the error labels for each joint. The error labels are the same as the error labels used in the data labelling explained in section 4.4. The fully connected layers of both networks use intermittent rectified linear unit (ReLU) activation functions to combat the vanishing gradient problem by passing only the values which are greater than zero into the next layer.

While FESDModelv1 uses the data as it is stored in the dataset, FESDModelv2 merges the data into a single RGB image. This is done using the feature extractor, which is trained on RGB images. The data is merged by assigning each modality to a channel in an RGB image. The RGB image is transformed into greyscale and assigned to the red channel, the

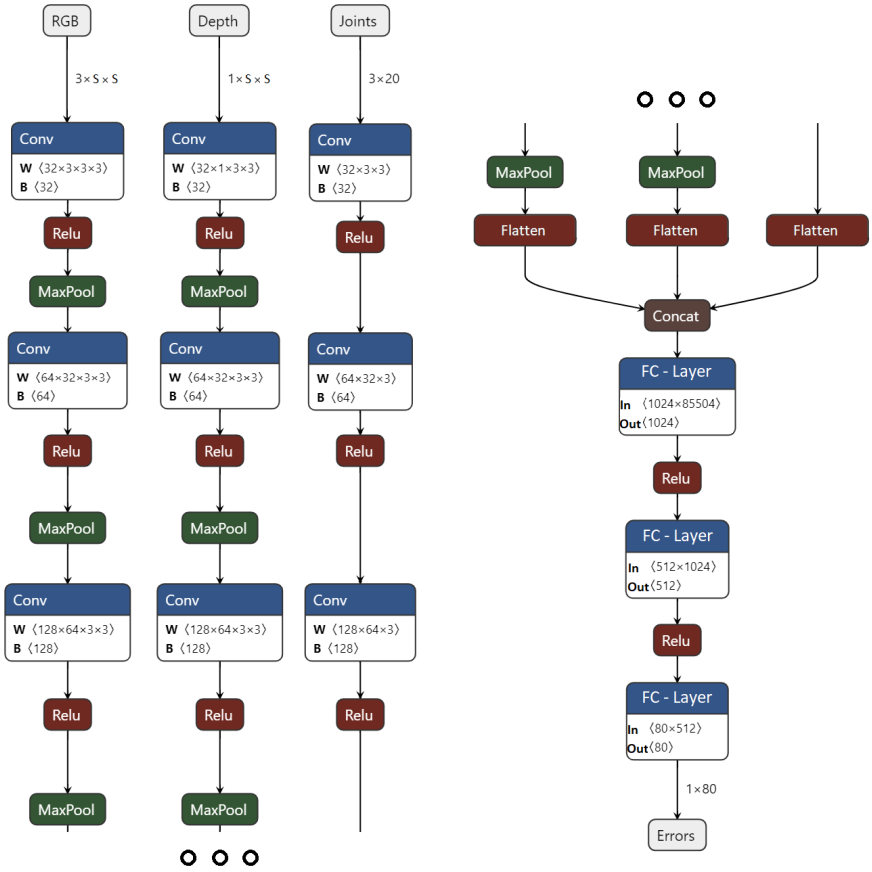

Figure 5-1: Original FESDModel architecture with three different inputs; RGB, Depth and Joint data. With 'S' as the image size. After three convolutions the three streams are concatenated to be passed into three fully connected layers with ReLU activation functions. In this example network, the model calculates the joint problem set, therefore the output is a 1D 80 tensor of multi-object, one for each joint, i.e. 20, multi-class, one for each error class, i.e. 4, values.

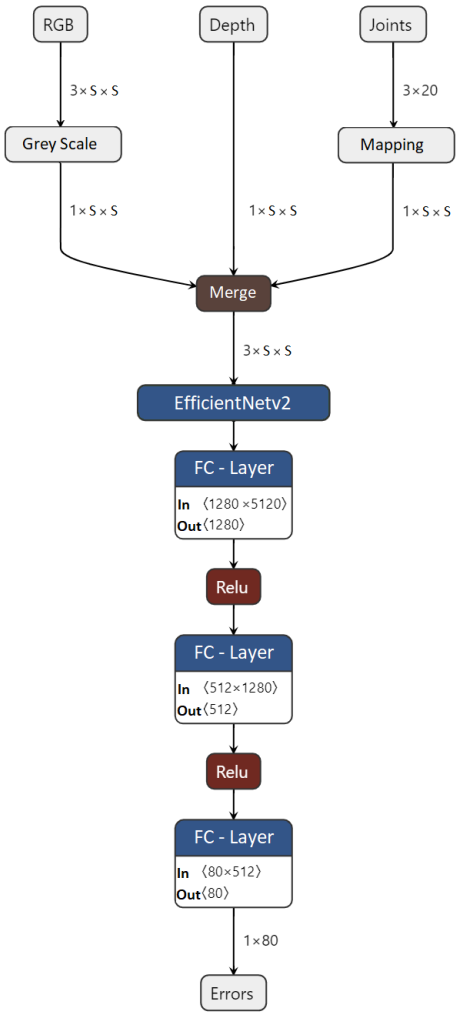

Figure 5-2: FESDModelv2 architecture with transfer learning. The input is merged into a single RGB image and passed into a feature extractor. With 'S' as the image size. The feature extractor is a pre-trained EfficientNet v2 S. The output of the feature extractor is passed into two fully connected layers with ReLU activation functions. In this example network, the model calculates the joint problem set, therefore the output is a 1D 80 tensor of multi-object, one for each joint, i.e. 20, multi-class, one for each of the 4 error classes.

depth image is scaled to a value between 0 and 255 and assigned to the green channel, and the joint coordinates are assigned to the blue channel.

In total eight models were developed and trained. Four models were trained using FESDModelv1 and four models were trained using FESDModelv2. Each of the models corresponds to one of the problem sets introduced in section 4.5, i.e. one model for each problem set is trained using FESDModelv1 and one model for each problem set is trained using FESDModelv2.

The output of the model varies depending on the problem set. The joint problem set contains more detailed error information, which was discussed in section 4.4. Therefore, the models developed to detect joint-level errors have an output vector of size 80, i.e. twenty joints, each with four different error labels. The other problem sets are labelled using two values to represent whether an area is faulty, "Error" or "No Error". Hence the Full Body, Half Body and Body Part problem sets have an output vector of size 2, 4, and 12 respectively.

To choose a network that is used by FESDModelv2 as a feature extractor, multiple different networks have been compared, which can be seen in figure 5-3. One of the target applications of the model is to be used in a real-time application so that error handling can be conducted. Consequently, a lightweight model which does not impact the performance much is preferred. Therefore, the models are compared by the number of floating-point operations (FLOPS) to their Accuracy on ImageNet-1K. Table 5.1 shows the top 5 models according to their accuracy and performance.

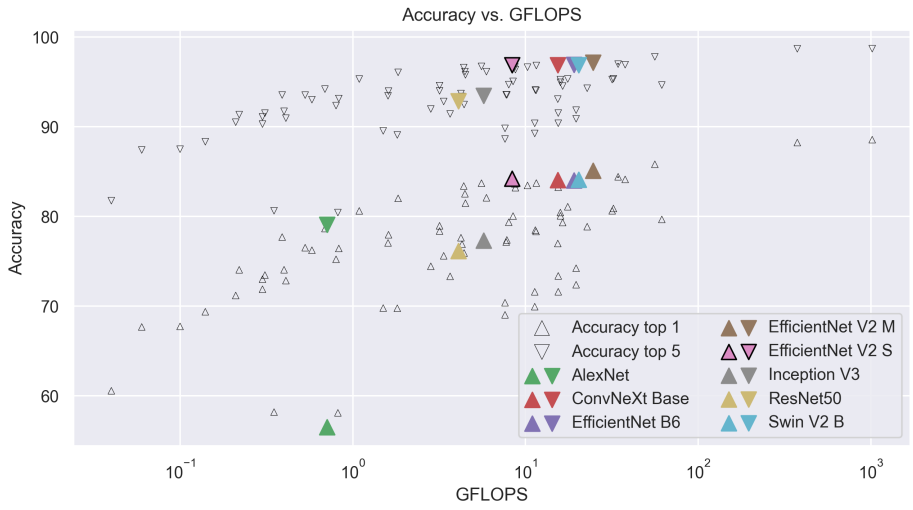

Figure 5-3: The comparison of different networks by their GFLOPS and their Top-5 Accuracy. The models are sorted by their GFLOPS and their Top-5 Accuracy[1]. The models are EfficientNet V2 S, ConvNeXt Base, EfficientNet B6, Swin V2 B, and EfficientNet V2 M. Additionally, AdamNet, ResNet-50 and Inception-v3 are added as a reference.

EfficientNet v2 was chosen since it proved to be the most performant while being the most accurate of the networks that were analysed. In particular, the small variant with 2.15×10^7 Parameters and a Top-1 Accuracy of 84.228%[27]. While EfficientNet V2 M outperforms EfficientNet V2 S in terms of Top-1 Accuracy, the number of additional parameters needed to achieve a better accuracy outway the performance bonus that EfficientNetv2 S brings with it. EfficientNetv2 is a convolutional neural network, which optimises training

Table 5.1: The top 5 models according to their accuracy and performance. The models are sorted by their GFLOPS and their Top-5 Accuracy[2]. The models are EfficientNet V2 S, ConvNeXt Base, EfficientNet B6, Swin V2 B, and EfficientNet V2 M.

Weight	Acc@1	Acc@5	Params	GFLOPs
EfficientNet V2 S	84.228	96.878	2.15×10^7	8.370
ConvNeXt Base	84.062	96.870	8.86×10^7	15.360
EfficientNet B6	84.008	96.916	4.30×10^7	19.070
Swin V2 B	84.112	96.864	8.79×10^7	20.320
EfficientNet V2 M	85.112	97.156	5.41×10^7	24.580

speed and parameter efficiency and improves upon EfficientNet[28]. The main focus of EfficientNet is the scaling of the model in width, depth and resolution of the input image.

5.2 Data preparation

To successfully train FESDModel three steps are taken before training can begin, data augmentation, data merging, and data balancing. The data augmentation is done to ensure that the model is robust to different variations in the data. The data merging is done to combine the different modalities into a single tensor. Since the dataset is unbalanced, the data balancing is done to ensure that the model is not biased toward any particular error label.

The finished data preparation pipeline for FESDModelv1 and FESDModelv2 can be seen in figure 5-4.

The joints are stored within a JSON file containing the coordinates of each joint in 2D and 3D. To process the 2D joint data is drawn on an image that has the same dimensions as the RGB and Depth image for FESDModelv2. For FESDModelv1 the position of each joint relative to the waist joint is passed into the network.

5.2.1 Data augmentation

Four different augmentations are applied to the data to generalise the data. The first augmentation is flipping the data. The RGB image, the depth image, and the joint image are flipped horizontally. Furthermore, the ground truth data is flipped, as labels refer to the left or right side of the body, which would no longer coincide with the data that is passed into the network.

Additionally, the images are cropped at random while keeping the positions of the joints and a margin around the joints visible. This ensures that the model is robust to different positions of the user in the image.

Finally, Gaussian noise is applied to the RGB image and the depth image. This further improves the robustness of irregular data.

The augmentations can be seen in figure 5-4 where they are applied to a sample frame from the dataset.

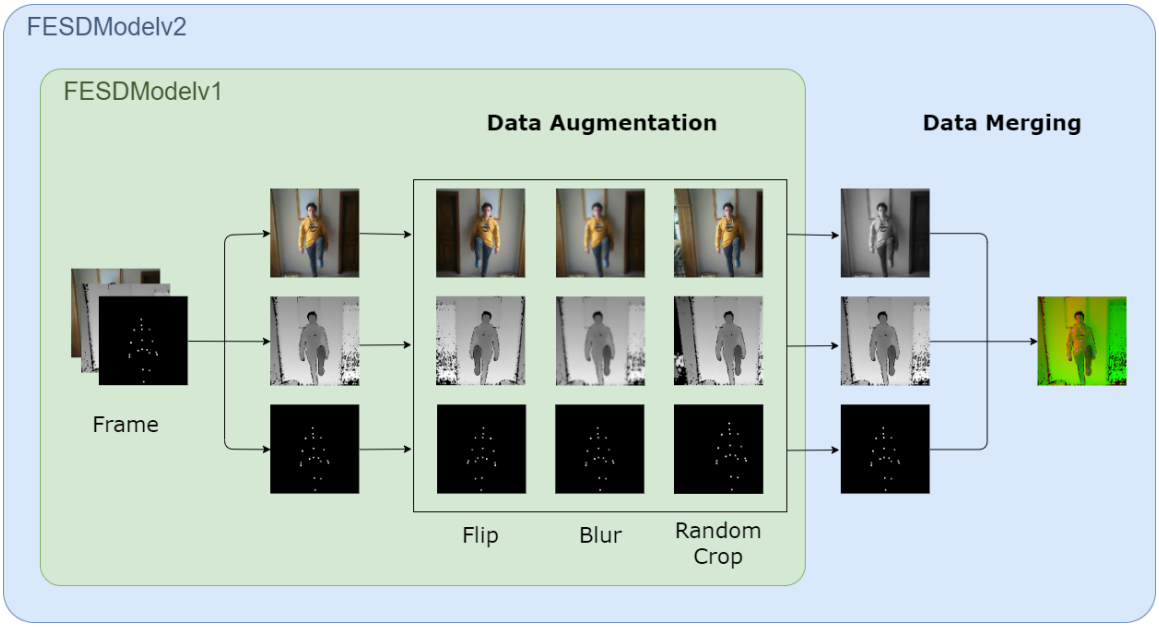

Figure 5-4: The three modalities are separately randomly flipped, Blurred, and Cropped. For FESDModelv1 the separate modalities are passed into the network. For FESDModelv2, the RGB image is transformed into a greyscale image and all three modalities are merged into a single RGB image.

5.2.2 Data balancing

In the ordinary case, HPE is not meant to produce faulty results. In the selected exercises it is aimed to produce faulty results. However, this does still not produce a balanced dataset. In section 4.7, the statistics of the dataset are shown. Most notably for the problem set *Half* and *Full*, in figures 4-8 and 4-7, where the error label *No Error* is overrepresented it can be seen that the dataset is imbalanced.

To balance the dataset, frames are sampled using a Weighted Random Sampler for each batch of the training. The weights for the samples are calculated based on the occurrence of the error labels in the dataset. While only considering the whole body as a single object, the calculation of the weights is simple. For each frame, the error label is counted and the inverse of the count is used as the weight for the frame. This ensures that the model is not biased toward any particular error label by oversampling the frames which contain an error.

However, for the other problem sets the calculation of the weights is more complex. In the other problem sets each frame contains an error for each area, e.g. when considering the Half-Body problem, the upper and lower body 2 errors. To successfully balance the dataset for each area four weights would need to be created and balanced, i.e. the upper and lower body have an error the upper body is faulty and the lower body is not, etc. This would oversample some frames while undersampling others. In the other problem sets this is far more visible. Therefore, it was decided to consider the sum of erroneous joints per frame as a balancing factor. This means that frames that have the same number of erroneous areas are weighed the same.

5.3 Experimental Setup

To train the models the data has to be passed into the network so that it can predict a value. Based on that value a loss is calculated which is used to adapt the weights of the networks. In the case of FESDModel *cross entropy loss* is used. In cases where the problem set contains more than one problem area, i.e. all problem sets except the full body problem set, the cross entropy loss is calculated for each object or area separately and a summed cross entropy loss is calculated.

Carl F. Sabottke and Bradley M. Spieler showed in their study that a lower resolution of the input images achieves better performances[29]. They found that images that were passed into a CNN which were of a resolution of 300x300 pixels achieved worse results than images with 64x64 pixels. Therefore, the images are scaled to 64x64 pixels.

Both networks are trained using the Adam optimiser, as described by Diederik P. Kingma and Jimmy Ba[30], with an initial learning rate of 0.00005 with learning rate decay.

To improve the performance of the training process Cuda is used. To further speed up the training a batch size of 32 is used.

Chapter 6

Results

In this chapter, the results of the experiments are presented. The results for each different problem set is presented seperatly.

6.1 FESDModelv1 Results

After training all four models using FESDModelv1, the results are evaluated. Table 6.1 shows the results of the testing after 50 epochs of training. The results seem promising with an accuracy in the range of 80 to 90 percent. Additionally, the Cohen's Kappa coefficient shows results in a good range.

Table 6.1: The test results of FESDModelv1 after 50 epochs of training. Showing the Percentage of Positive Guesses (PPG), the Accuracy (Acc), the F-β score calculated with $\beta = [1, 0.5, 2]$ (F1, F0.5, F2 respectively) and the Cohen's Kappa Coefficient (κ).

Problem Set	PPG	Acc	F1	F0.5	F2	κ
Full Body	50.42	0.69	0.75	0.84	0.67	0.37
Half Body	55.83	0.77	0.79	0.80	0.79	0.53
Body Parts	79.03	0.78	0.87	0.89	0.84	0.22
Joints	70.00	0.89	0.91	0.91	0.92	0.77

To get a further understanding of these results the cofusion matrix and ROC curve were calculated. The confusion matrices can be seen in figure 6-1 and ROC curves can be seen in figure 6-2.

The odd looking figure 6-2d can be explained using the results of the prediction. The model predicting the joint problem set is overconfident and therefore, there is only a limited number of thresholds that can be shown in the ROC curve. Therefore, the majority of the datapoints is in the upper right corner.

The model is most accurate when predicting the body part problem set according to the calculated F1 score. However, there is a discrepancy between the F1 score, which is around 0.87, and Cohen's Kappa metric, which is only around 0.22. The reason for this discrepancy can be seen when considering the confusion matrix for each of the body parts.

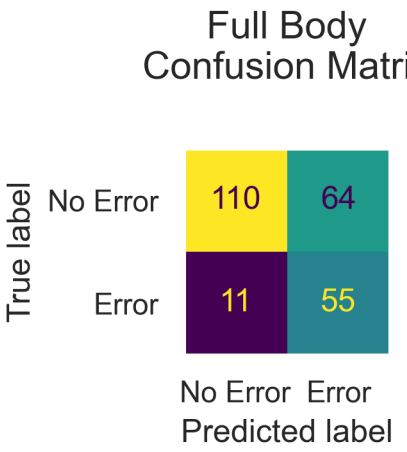

(a) Full Body Problem Set

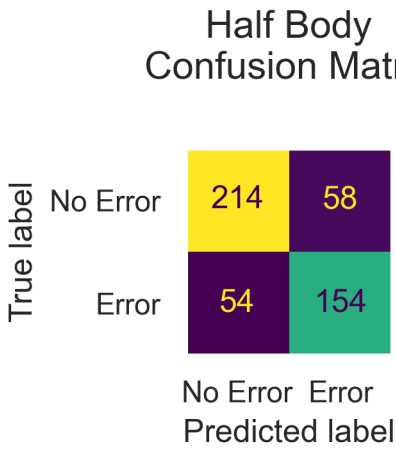

(b) Half Body Problem Set

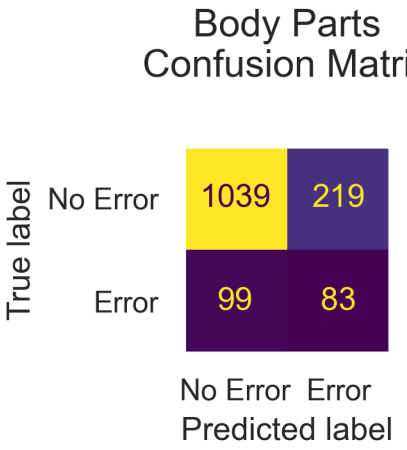

(c) Body Part Problem Set

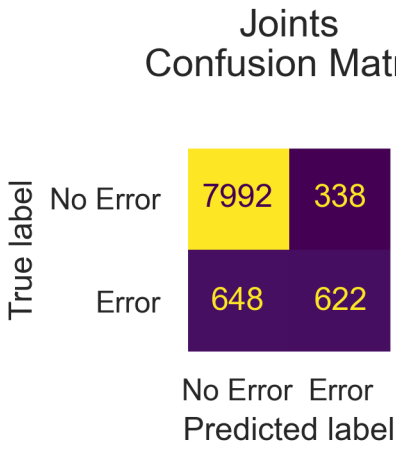

(d) Joint Problem Set

Figure 6-1: The confusion Matrices of FESDModelv1.

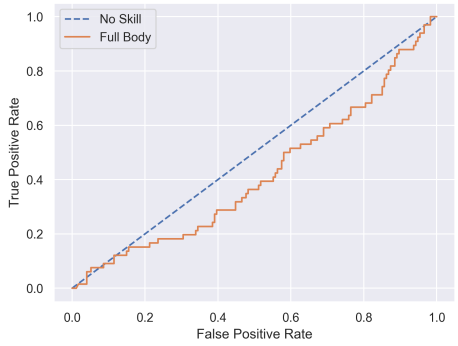

(a) Full Body Problem Set

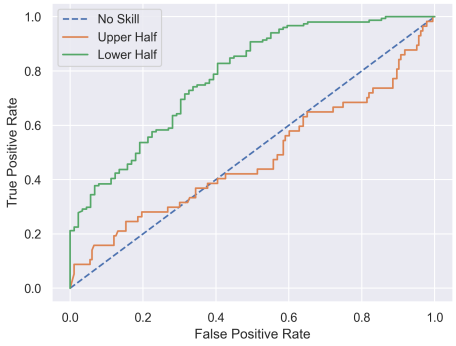

(b) Half Body Problem Set

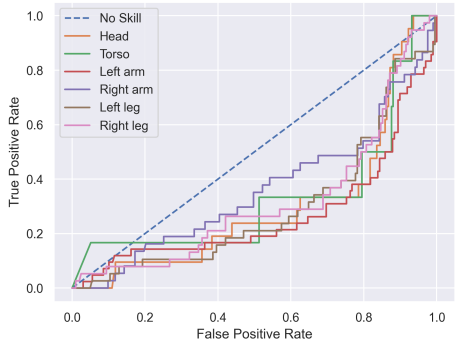

(c) Body Part Problem Set

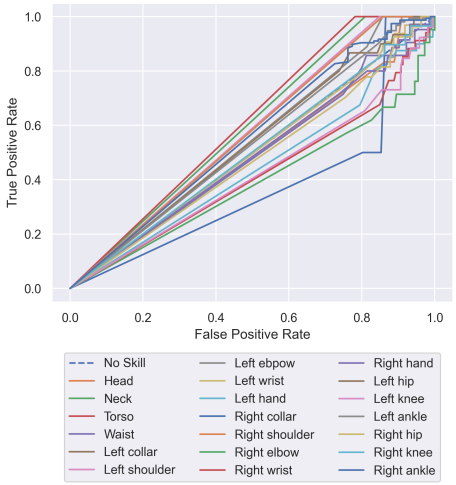

(d) Joint Problem Set

Figure 6-2: The ROC curves of FESDModelv1.

This can be seen in figure 6-3. While the model predicts that there is no error quite well, it does not predict errors well.

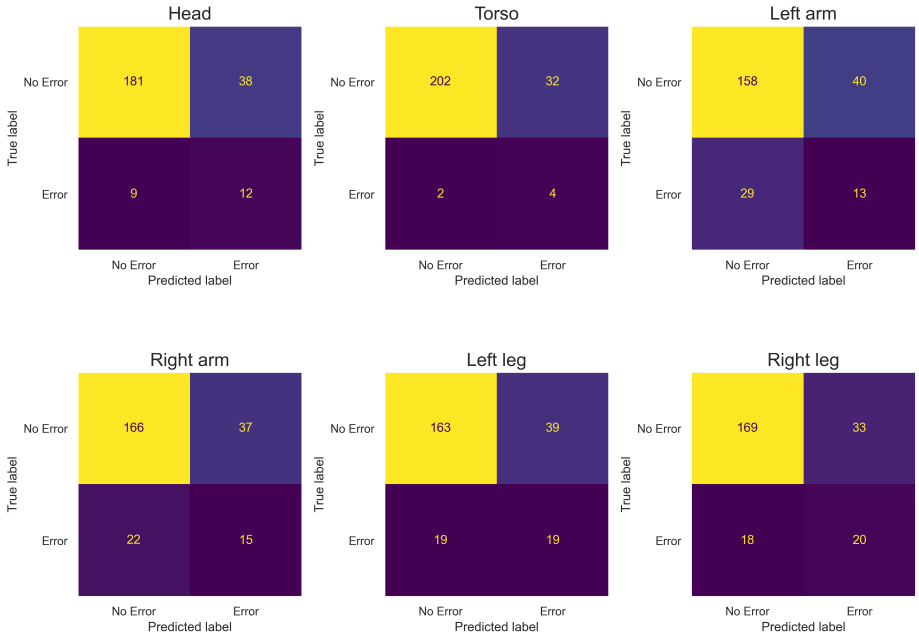

Figure 6-3: The confusion matrix of each body part for FESDModelv1 for the body part problem set.

When only considering the accuracy of FESDModelv1 when predicting the joint problem set, it seems that FESDModelv1 is predicting the error labels well. However, since the results are taken as the average the individual results have to be investigated to get a clear picture of the results. Figure 6-4 shows the confusion matrix of each joint on the test dataset. It can be seen that each joint is only predicting either no error or error depending on the joint. This is probably due to the unbalanced nature of the dataset.

The best results are achieved using the half-body problem set. In Figure 6-5 the confusion matrix for the upper and lower body can be seen. The matrices indicate that FESDModelv1 is more accurate when detecting errors for the lower body than for the upper body. This is also reflected by the ROC-Curve seen in figure 6-2b, which shows that the lower body is achieving better results than the upper body.

Figure 6-4: The confusion matrix of each joint for FESDModelv1 for the joint problem set.

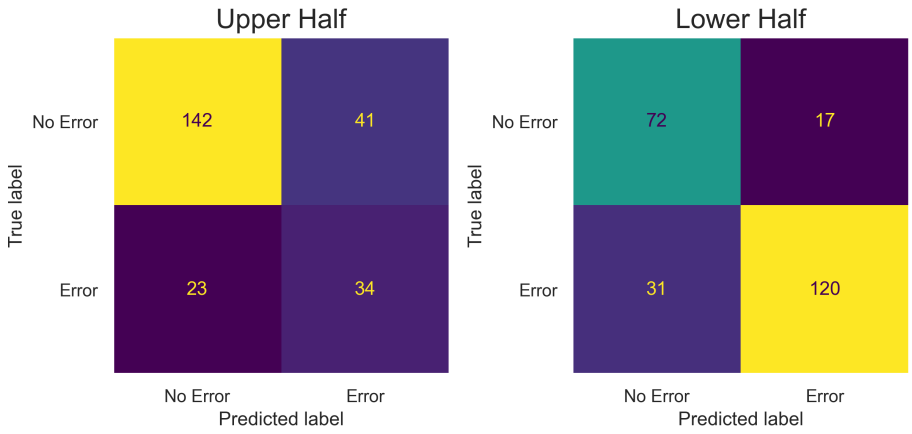

Figure 6-5: The confusion matrix of the upper and lower body for FESDModelv1 for the body half problem set.

6.2 FESDModelv2 Results

The results of the testing after 50 epochs of training for FESDModelv2 can be seen in table 6.2. The numeric values of the accuracy and F1-Score show good results. However, the percentage of positive guesses metric seems to hint at overfitting.

Table 6.2: The test results of FESDModelv2 after 50 epochs of training. Showing the Percentage of Positive Guesses (PPG), the Accuracy (Acc), the F-β score calculated with $\beta = [1, 0.5, 2]$ (F1, F0.5, F2 respectively) and the Cohen's Kappa Coefficient (κ).

Problem Set	PPG	Acc	F1	F0.5	F2	κ
Full Body	97.92	0.70	0.83	0.76	0.91	-0.04
Half Body	61.25	0.71	0.76	0.74	0.77	0.41
Body Parts	100.00	0.87	0.93	0.90	0.97	0.00
Joints	69.99	0.89	0.91	0.91	0.92	0.77

The results shown in table 6.2 are reflected in the confusion matrices seen in figure 6-6. The half-body and body parts problem set only guess positive results, hence the Percentage of positive guesses. The Cohen's Kappa Coefficient is 0 if $tp \cdot tn = fn \cdot fp$. This is the case if only one class is guessed, which is the case if all guesses are positive.

The ROC-curves shown in figure 6-7, show the different true positive and false positive rates for each of the areas in each problem set.

The Joint model seems like it is getting good results when considering all joints together. However, when considering the confusion matrix for each of the joints, as can be seen in figure 6-8, the show that while in total not a single error label is guessed all the time for all joints together, each joint does not have varying error labels and is therefore not a good model.

Similar to FESDModelv1, the Half Body problem set is getting very good results which do not indicate overfitting. In figure 6-9 the confusion matrices can be seen for the upper

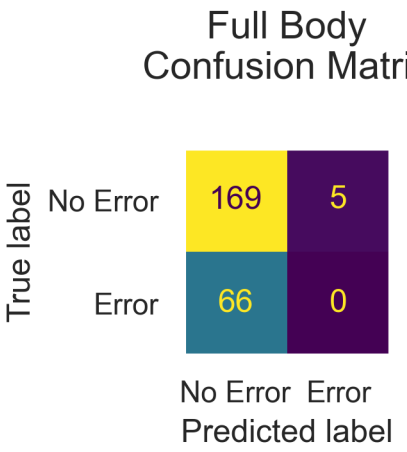

(a) Full Body Problem Set

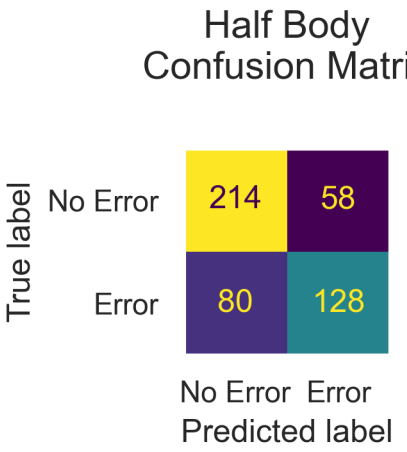

(b) Half Body Problem Set

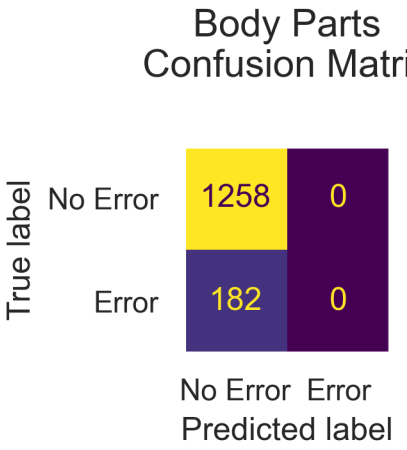

(c) Body Part Problem Set

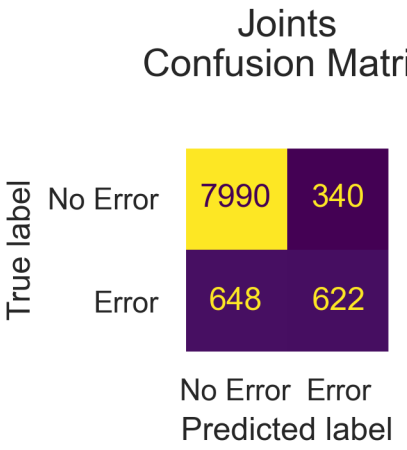

(d) Joint Problem Set

Figure 6-6: The confusion Matrices of FESDModelv2.

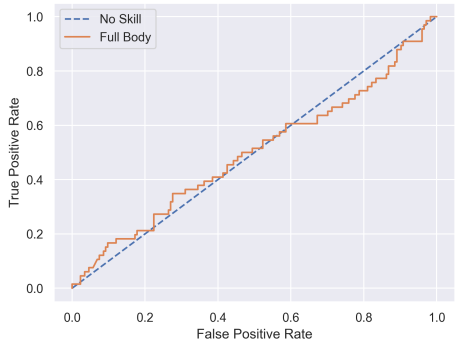

(a) Full Body Problem Set

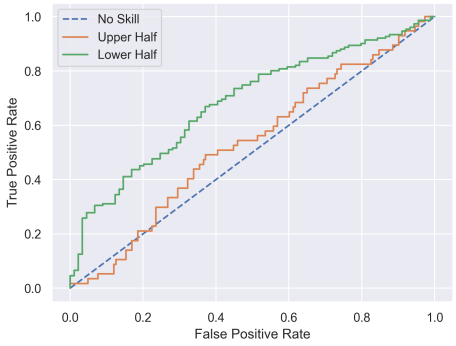

(b) Half Body Problem Set

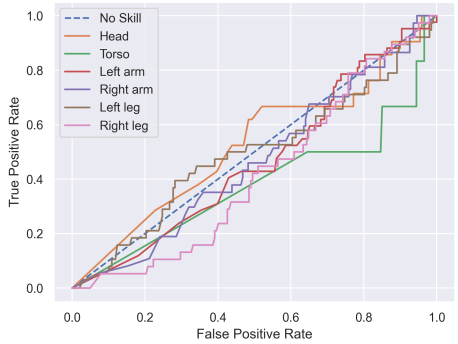

(c) Body Part Problem Set

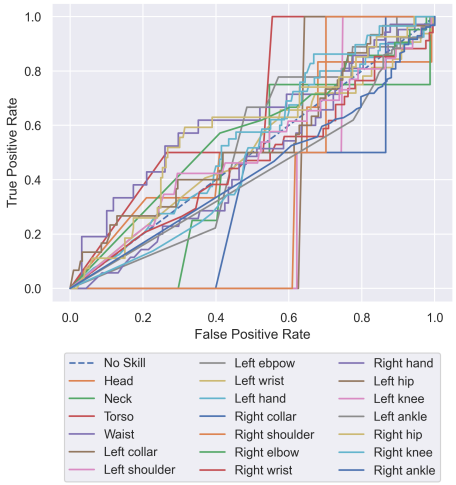

(d) Joint Problem Set

Figure 6-7: The ROC curves of FESDModelv2.

Figure 6-8: The confusion matrix of each joint for FESDModelv2 for the joint problem set.

and lower body. It can be seen that the detection of the lower body is more successful than the detection of the upper body. It is important to consider, that the upper body has far more stable joints and more joints in general. This discrepancy might be the reason for the diverging accuracy of the upper and lower body.

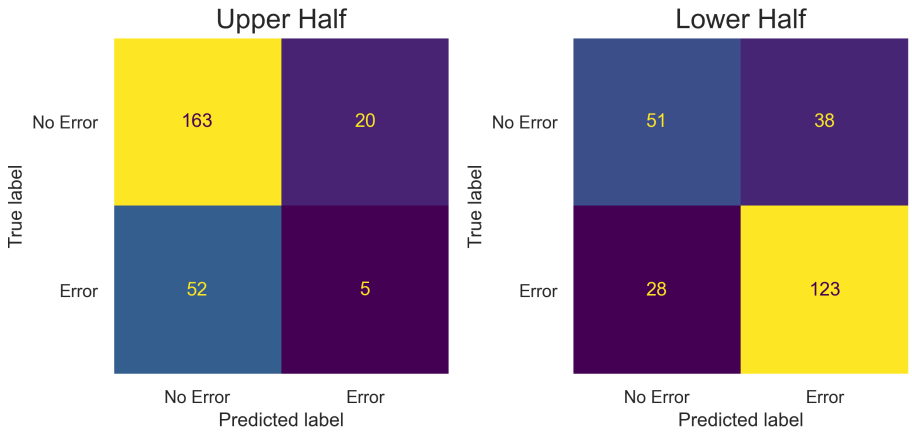

Figure 6-9: The confusion matrix of the upper and lower body for FESDModelv2 for the body half problem set.

Chapter 7

Conclusion

In order to improve on existing human pose estimators we have to understand the errors and how they occur. In the scope of this thesis, the following research questions were asked; (A) What errors occur during HPE and how can these errors be reproduced in a controlled manner? (B) How can a dataset of multiple modalities be captured, to analyse if the previous observations about problems during pose estimation are correct? (C) How can the previously captured and labelled dataset be used to train a model using multi-modal data to determine if a joint is faulty or not?

A Common problems of HPE were analysed and exercises were designed that cause issues in a controlled manner. It was found that lighting has a high influence on the pose estimation, as well as the posture of the user, and the visibility of the head.

B Using these exercises a dataset, FESDDataset, was captured and labelled using a custom tool for multi-modal stream capture and error labelling for HPE, FESDData. To investigate different problem areas were defined four different problem sets that encompass different abstractions of the problem.

C Finally, two different models were conceptualised as preliminary experiments which use different methods to process the different modalities. FESDModelv1 extracts the features of each modality individually, whereas FESDModelv2, combines all three modalities into a single RGB image, which is passed into a pre-trained model for feature extraction.

The result of preliminary experiments showed that both FESDModelv1 and FESDModelv2 achieve the best results with the half body problem set, in which the upper and lower halves can individually be detected as faulty. In general, FESDModelv1 seems to outperform FESDModelv2 for every problem set. This might be due to the feature extraction method. While EfficientNet performs very well on standard RGB images it was not trained on the merged modalities as they were used by FESDModelv2. All in all, the preliminary experiments can be considered as successful, as it was proven that the development of a model for error detection is possible. However, more data is necessary to avoid overfitting of the models and to form a more generalised method.

7.1 Contribution

In this thesis, Exercises were proposed, which challenge HPE at varying difficulties. Furthermore, a database collection tool, FESDData was developed, which allows the capture of RGB, Depth and Pose data simultaneously and allows for the labelling of errors. Using that tool FESDDataset was captured which contains 300 frames for 13 Exercises which were recorded twice, resulting in a total of 7800 frames of multimodal data. Finally, preliminary experiments were conducted to show the viability of model development on the recorded data.

The code of this thesis is available on GitHub[1]. The repository is divided into two major parts, FESDData, which contains the C++ implementation of FESDData, FESDModel, which contains the implementation of the model, FESDModelv1 and FESDModelv2, as well as the Jupyter notebooks that were used to evaluate the dataset, to train and evaluate the model. FESDDataset, as well as the trained models, are available on request.

7.2 Future work

To further improve the dataset and the model, FESDData and FESDDataset could be expanded to include the accurate position of the joints in the image. This would allow for the use of the dataset for error correction.

To improve the quality of the FESDModel, more data needs to be collected and labelled in different settings. The current dataset is limited to a single room with a single camera. To improve the model, the dataset needs to be expanded to include different scenes, different pieces of clothing and different camera angles. These additions might prevent the model from overfitting. Additionally, the model could be improved by using a different backbone, which is not as performant but more accurate, such as EfficientNet v2 M.

7.2.1 Possible applications

FESD might find several different areas of application in the future. Firstly, the trained model can be used to assist in developing games and other applications that utilise HPE. In its simplest application, it may be used to warn users of possible errors when the skeleton is not detected correctly. In more advanced cases the information provided by the model could be used to attempt to fix joints through joint position interpolation and prediction rather than using the faulty joint. Moreover, multiple human pose estimators could be considered resulting in an overall more robust HPE.

Furthermore, if the model proves to have high accuracy for a specific use case, it could be used to train a better pose detector in the same way as it is proposed by João Carreira et al.[10].

The dataset and the dataset recorder may also be used to further the development of FESDModel and it can also find application in other areas such as recording datasets for action recognition. The dataset in and of itself can be used for action detection. The exercises are predefined and can be recorded and automatically labelled by FESDData, thereby making it easy to record large amounts of data without requiring manual labelling.

[1] https://github.com/LeonardoPohl/FESD

In conclusion, while the models that were developed in the scope of the thesis proved to be overfitting, the foundational work of the error assessment and FESDData can prove useful for future research in the area of error detection of HPE, which is an area with very limited research.

References

[1] L. Kumarapu and P. Mukherjee, "AnimePose: Multi-person 3D pose estimation and animation," *Graphics*, 2020.

[2] K. Chen, P. Gabriel, A. Alasfour, C. Gong, W. K. Doyle, O. Devinsky, D. Friedman, P. Dugan, L. Melloni, T. Thesen, D. Gonda, S. Sattar, S. Wang, and V. Gilja, "Patient-Specific Pose Estimation in Clinical Environments," *IEEE Journal of Translational Engineering in Health and Medicine*, vol. 6, pp. 1–11, 2018.

[3] B. Preim and M. Meuschke, "A survey of medical animations," *Computers and Graphics*, vol. 107, 09 2022.

[4] F. Kröger, *Automated Driving in Its Social, Historical and Cultural Contexts*, pp. 41–68. Springer, 05 2016.

[5] J. Stenum, K. M. Cherry-Allen, C. O. Pyles, R. Reetzke, M. F. Vignos, and R. T. Roemmich, "Applications of Pose Estimation in Human Health and Performance across the Lifespan," *Sensors (Basel, Switzerland)*, vol. 21, 2021.

[6] M. Tölgyessy, M. Dekan, and L. Chovanec, "Skeleton Tracking Accuracy and Precision Evaluation of Kinect V1, Kinect V2, and the Azure Kinect," *Applied Sciences*, vol. 11, p. 5756, 06 2021.

[7] Z. Cao, G. Hidalgo Martinez, T. Simon, S. Wei, and Y. A. Sheikh, "OpenPose: Realtime Multi-Person 2D Pose Estimation using Part Affinity Fields," *IEEE Transactions on Pattern Analysis and Machine Intelligence*, 2019.

[8] T. Simon, H. Joo, I. Matthews, and Y. Sheikh, "Hand Keypoint Detection in Single Images using Multiview Bootstrapping," in *CVPR*, 2017.

[9] Z. Cao, T. Simon, S.-E. Wei, and Y. Sheikh, "Realtime Multi-Person 2D Pose Estimation using Part Affinity Fields," in *CVPR*, 2017.

[10] J. Carreira, P. Agrawal, K. Fragkiadaki, and J. Malik, "Human Pose Estimation with Iterative Error Feedback," *CVPR*, 2015.

[11] Y. Li, R. Bu, M. Sun, W. Wu, X. Di, and B. Chen, "Pointcnn: Convolution on $\mathcal{X}$-transformed points," *CVPR*, 2018.

[12] A. Geiger, P. Lenz, and R. Urtasun, "Are we ready for autonomous driving? the kitti vision benchmark suite," in *Conference on Computer Vision and Pattern Recognition (CVPR)*, 2012.

[13] C. Ionescu, D. Papava, V. Olaru, and C. Sminchisescu, "Human3.6M: Large Scale Datasets and Predictive Methods for 3D Human Sensing in Natural Environments," *IEEE Transactions on Pattern Analysis and Machine Intelligence*, vol. 36, pp. 1325–1339, jul 2014.

[14] B. Seddik, S. Gazzah, and N. Essoukri Ben Amara, "Human-action recognition using a multi-layered fusion scheme of Kinect modalities," *IET Computer Vision*, vol. 11, no. 7, pp. 530–540, 2017.

[15] M. Fisch and R. Clark, "Orientation Keypoints for 6D Human Pose Estimation," *CVPR*, 2020.

[16] Y. Liu, "Contour Model and Robust Segmentation based Human Pose Estimation in Images and Videos," *International Journal of Signal Processing, Image Processing and Pattern Recognition*, vol. 8, pp. 1–10, 03 2015.

[17] Y. Chen, Y. Tian, and M. He, "Monocular human pose estimation: A survey of deep learning-based methods," *Computer Vision and Image Understanding*, vol. 192, p. 102897, 2020.

[18] M. Andriluka, L. Pishchulin, P. Gehler, and B. Schiele, "2D Human Pose Estimation: New Benchmark and State of the Art Analysis," in *IEEE Conference on Computer Vision and Pattern Recognition (CVPR)*, June 2014.

[19] T.-Y. Lin, M. Maire, S. Belongie, L. Bourdev, R. Girshick, J. Hays, P. Perona, D. Ramanan, C. L. Zitnick, and P. Dollár, "Microsoft COCO: Common Objects in Context," 2014.

[20] L. Sigal, A. Balan, and M. Black, "HumanEva: Synchronized Video and Motion Capture Dataset and Baseline Algorithm for Evaluation of Articulated Human Motion," *International Journal of Computer Vision*, vol. 87, pp. 4–27, 03 2010.

[21] S. An, Y. Li, and U. Ogras, "mRI: Multi-modal 3D Human Pose Estimation Dataset using mmWave, RGB-D, and Inertial Sensors," *CVPR*, 2022.

[22] V. Ganapathi, C. Plagemann, D. Koller, and S. Thrun, "Real time motion capture using a single time-of-flight camera," in *2010 IEEE Computer Society Conference on Computer Vision and Pattern Recognition*, pp. 755–762, 2010.

[23] V. Ganapathi, C. Plagemann, D. Koller, and S. Thrun, "Real-Time Human Pose Tracking from Range Data," in *Proceedings of the European Conference on Computer Vision (ECCV)*, 2012.

[24] J. Deng, W. Dong, R. Socher, L.-J. Li, K. Li, and L. Fei-Fei, "ImageNet: A large-scale hierarchical image database," in *2009 IEEE Conference on Computer Vision and Pattern Recognition*, pp. 248–255, 2009.

[25] C. Lee, "The roc space for a "better" and "worse" classifier.." Wikipedia, June 2018.

[26] M. McHugh, "Interrater reliability: The kappa statistic," *Biochemia medica : časopis Hrvatskoga društva medicinskih biokemičara / HDMB*, vol. 22, pp. 276–82, 10 2012.

[27] M. Tan and Q. V. Le, "Efficientnetv2: Smaller models and faster training," *CVPR*, 2021.

[28] M. Tan and Q. V. Le, "Efficientnet: Rethinking model scaling for convolutional neural networks," 2020.

[29] C. F. Sabottke and B. M. Spieler, "The Effect of Image Resolution on Deep Learning in Radiography," *Radiology: Artificial Intelligence*, vol. 2, no. 1, p. e190015, 2020. PMID: 33937810.

[30] D. P. Kingma and J. Ba, "Adam: A Method for Stochastic Optimization," in *3rd International Conference on Learning Representations, ICLR 2015, San Diego, CA, USA, May 7-9, 2015, Conference Track Proceedings*, 2017.

Appendix A

FESDData Appendix: Distribution of the number of joints with an error

Each problem set, except the joint problem set, is an abstraction from the base data which combines different areas of the pose into separate objects. A threshold is used to determine whether an area is considered as faulty based on the number of joints that are faulty in the pose. To determine this threshold the distribution of joints with errors is calculated for each of the problem areas over all the data and the 50th percentile is picked as the threshold.

Full Body problem set The results of the full body problem set can be seen in Figure A-1. The threshold is at two errors, i.e. if more than two joints in the whole body are faulty, the whole body is considered as faulty.

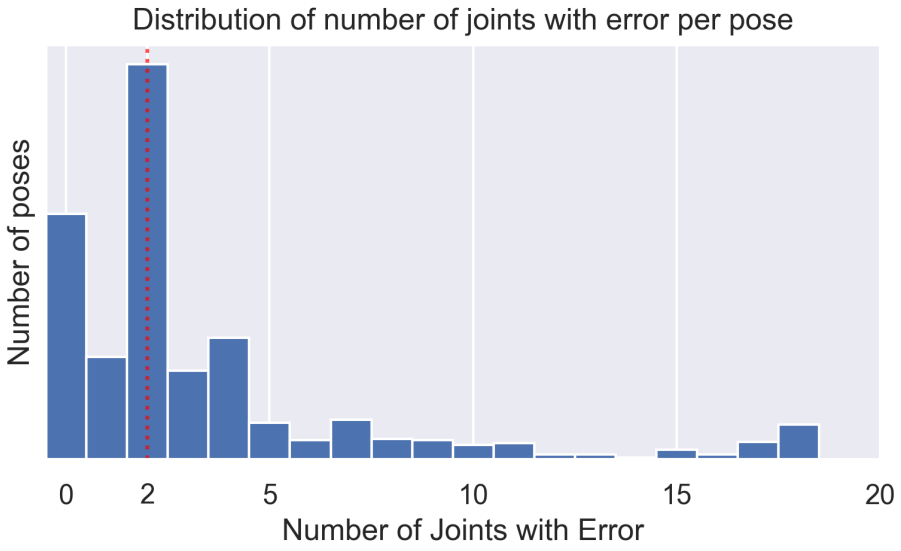

Figure A-1: The distribution of the number of joints with errors in each frame.

Half Body problem set The distribution of joints with errors for both the lower and upper body can be seen in figure A-2. If one joint in the upper body or more than two joints in the lower body are considered as faulty, the upper or lower body is considered as faulty respectively.

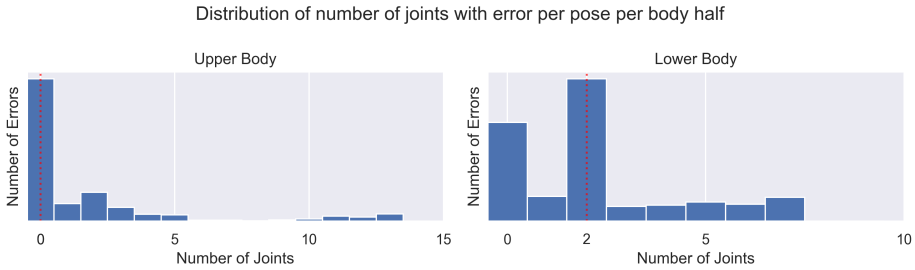

Figure A-2: The distribution of the number of joints with errors in each frame per body half.

Body parts problem set The left and right Legs require two or more faulty joints. Whereas all other body parts require only one or more errors to be considered as faulty.

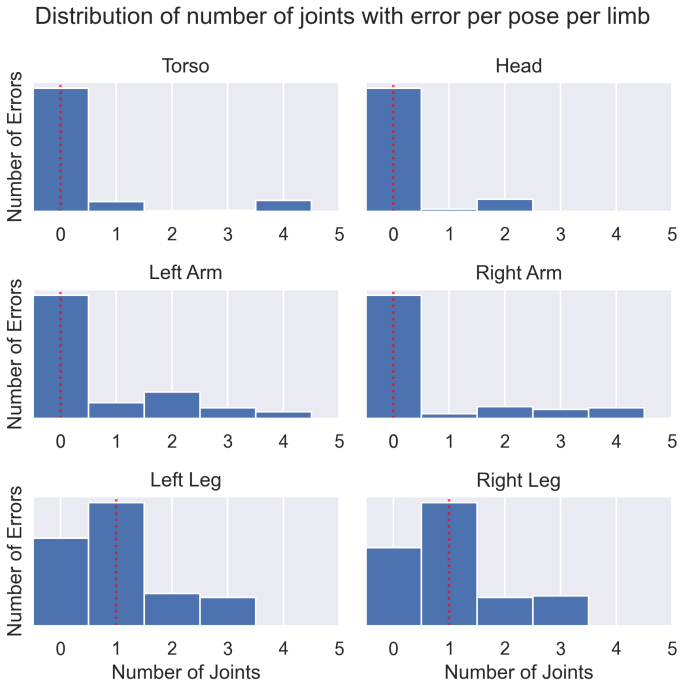

Figure A-3: The distribution of the number of joints with errors in each frame per body part.

Appendix B

FESDData Appendix: Distribution of Errors

This section contains the different distributions of errors for each of the problem sets.

Full Body Figure B-1 gives an overview of the error distribution by the difficulty of the exercise. The figure indicates that the difficulty of the exercise directly influences the percentage of errors that occur.

Figure B-1: The distribution of Errors of the full body problem set by difficulty.

Half Body The distribution of errors by difficulty for the half body problem set can be seen in figure B-2. Easy exercises seem to be less error-prone when grouping the joints into

body halves. This might be caused by the error threshold that was set before.

Figure B-2: The distribution of Errors of the half body problem set by difficulty.

Body parts The distribution of errors by difficulty can be seen in figure B-3. A less distinct distribution of errors can be seen when grouping the joints into body parts. Only a very small amount of errors occur during trivial exercises. This might be caused by the error threshold that was set before. The majority of errors occurring during trivial exercises are caused by a single faulty joint in the ankle. In Figure A-3 it is shown that the legs have an error threshold of two faulty joints. This means that the legs are considered faulty if there are more than two faulty joints. The ankle is the only joint that is faulty in trivial exercises. This means that the legs are not considered faulty.

Joints In medium exercises, the majority of errors that occur for the joints problem set, occur due to missing joints, rather than joints which are in the wrong position. This is shown in figure B-4.

A clear distinction between error-prone and stable joints can be seen in figure B-5. While in the majority of cases (72.3%) the right ankle is faulty only 4.9% of the left shoulder is faulty. Furthermore, the left and right ankles have a significant number of missing joints, contrary to the other joints, which have a more balanced distribution of error classes. This might be caused by occlusion or a cutoff from the image or a confidence which is too low and therefore discarded by Nuitrack.

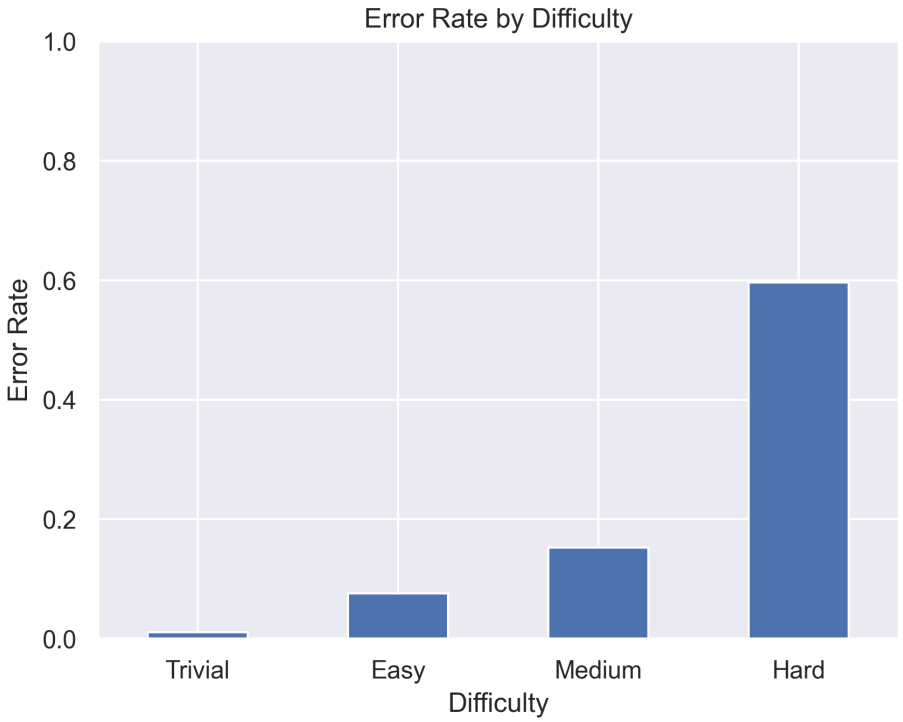

Figure B-3: The distribution of Errors of the half-body problem set by difficulty.

Figure B-4: The distribution of each error class grouped by difficulty.

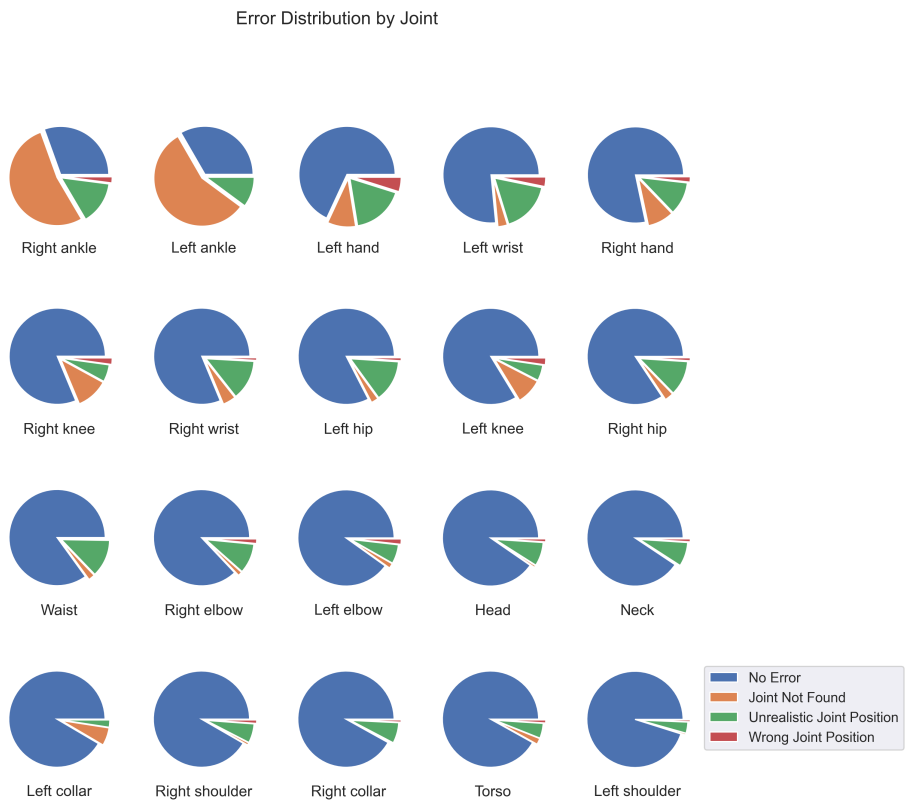

Figure B-5: The distribution of each error class grouped by joint.

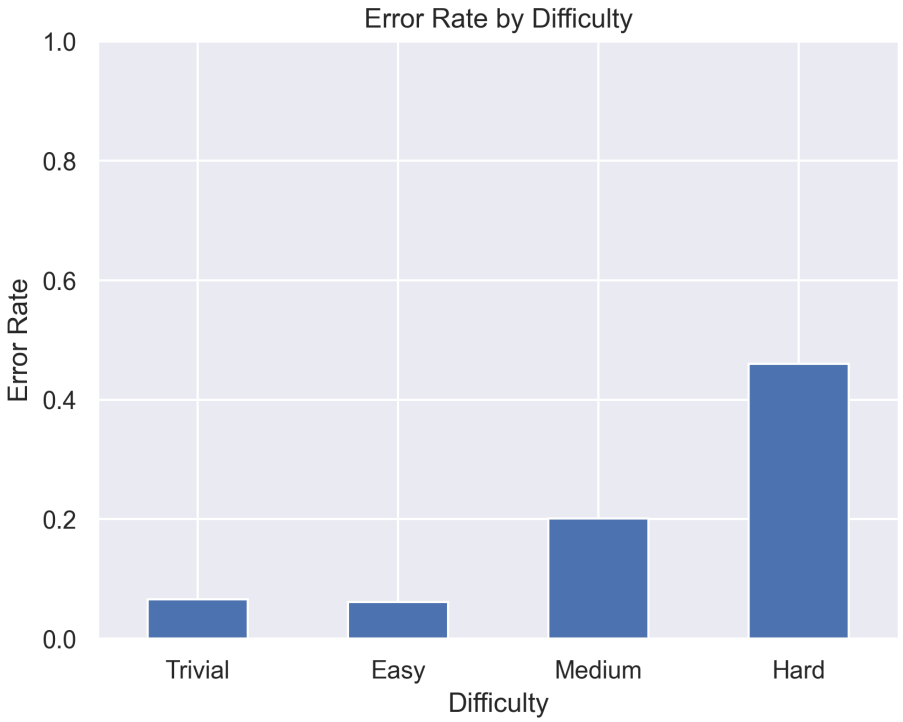

Figure B-6: The distribution of Errors of the joint problem set by difficulty.

Appendix C

Additional Results for FESDModelv1

In the figures C-1, D-2, D-5 and C-9, the training and test progress over all epochs can be seen.

Figure C-1: The training results of the full body model.

The figures C-11, C-13 and **??** show the confusion matrix divided by difficulty for all four problem sets.

(a) Upper Body Error Estimation

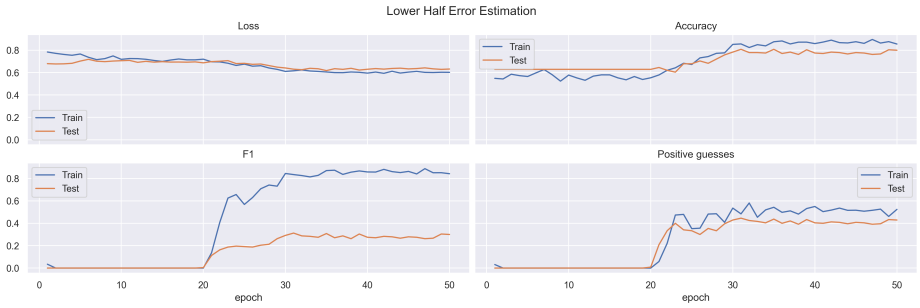

(b) Lower Body Error Estimation

Figure C-2: The training results of the half body error estimation model.

(a) Head Error Estimation

(b) Torso Error Estimation

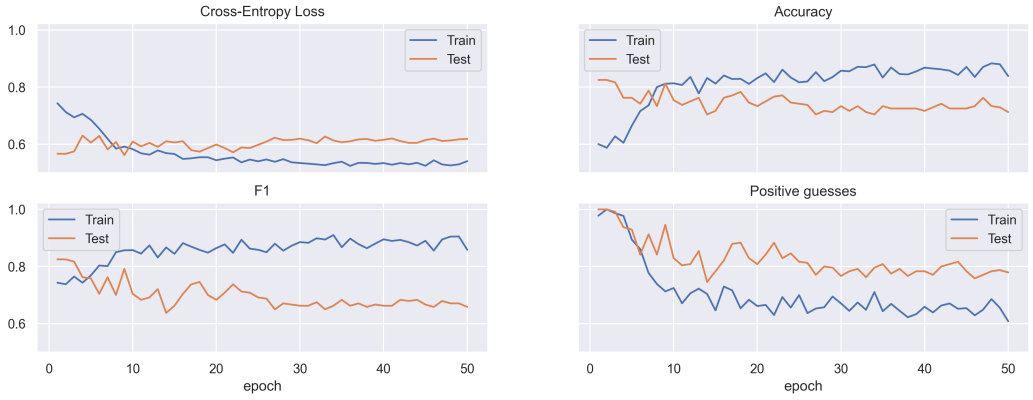

(c) Left Arm Error Estimation

(a) Right Arm Error Estimation

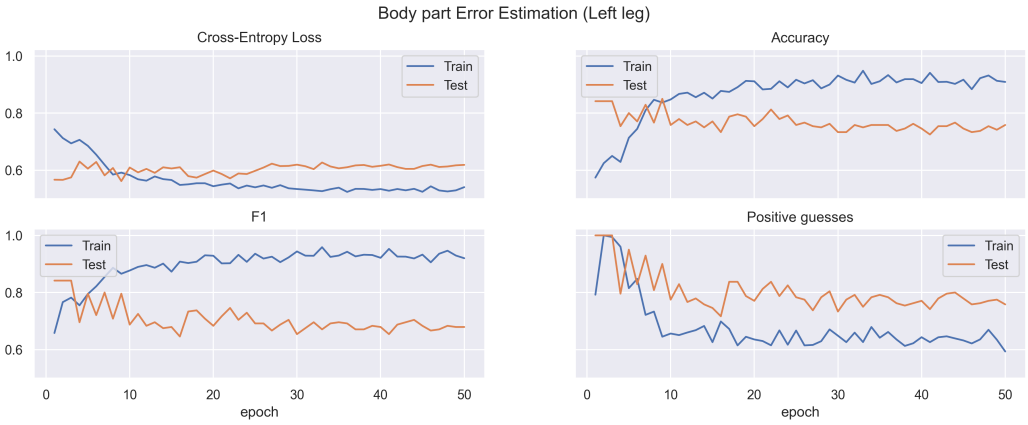

(b) Left leg Error Estimation

(c) Right leg Error Estimation

Figure C-4: The training results of the body part error estimation model.

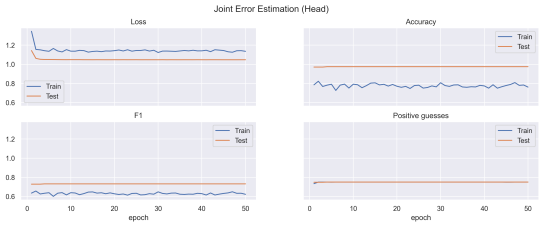

(a) Head Error Estimation

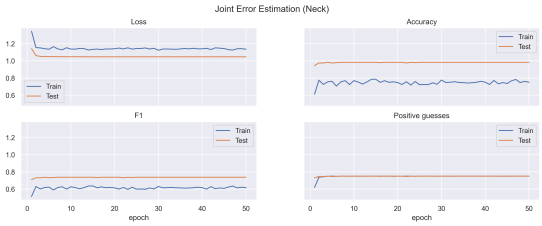

(b) Neck Error Estimation

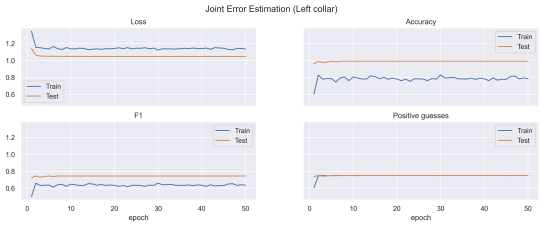

(c) Left Collar Error Estimation

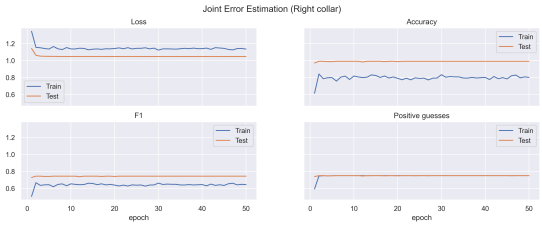

(d) Right Collar Error Estimation

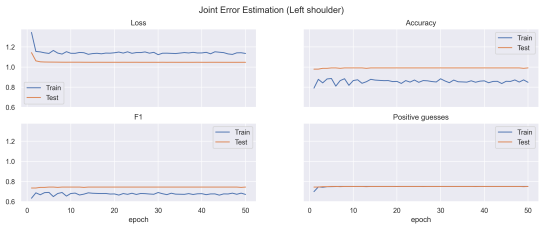

(a) Left Shoulder Error Estimation

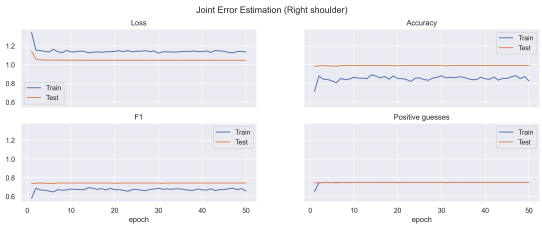

(b) Right Shoulder Error Estimation

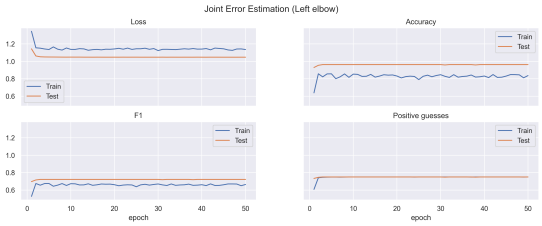

(c) Left Elbow Error Estimation

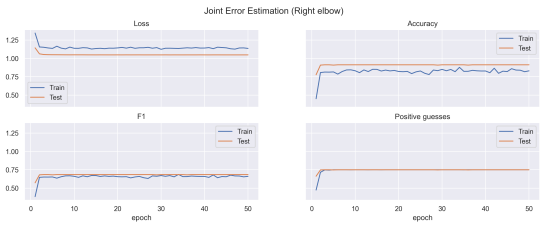

(d) Right Elbow Error Estimation

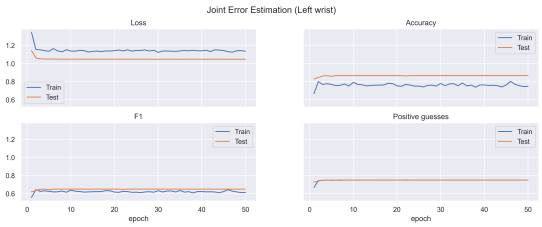

(a) Left Wrist Error Estimation

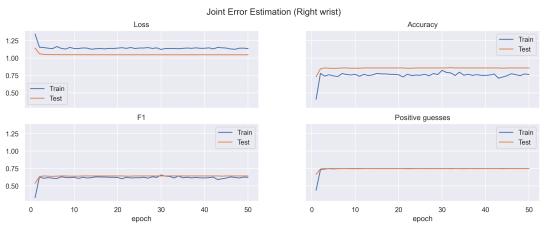

(b) Right Wrist Error Estimation

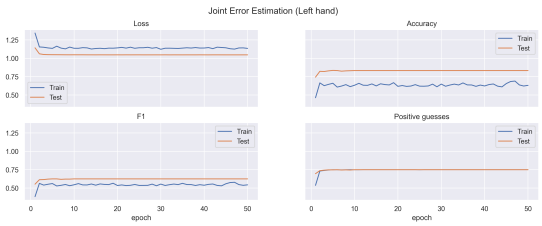

(c) Left Hand Error Estimation

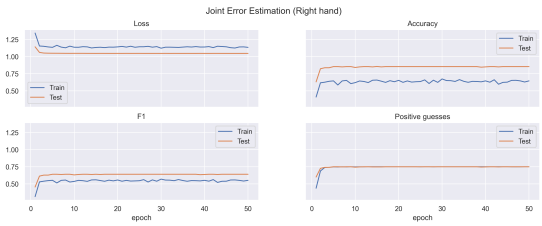

(d) Left Arm Error Estimation

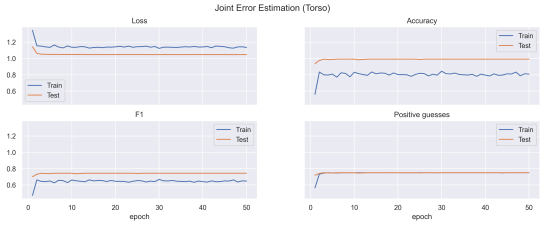

(a) Torso Error Estimation

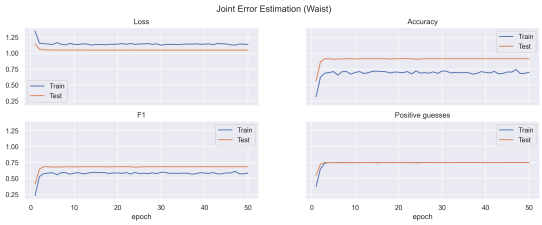

(b) Waist Error Estimation

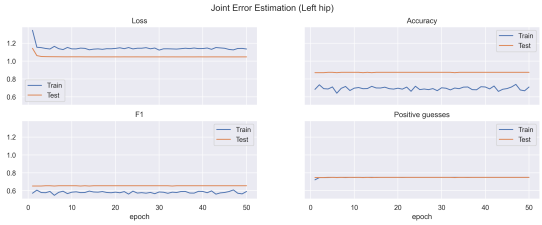

(c) Left Hip Error Estimation

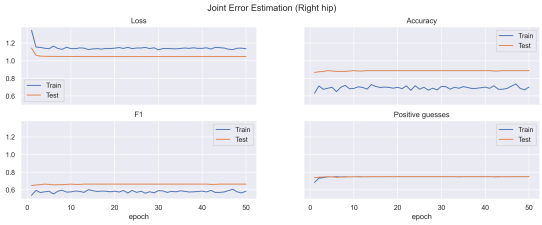

(d) Right hip Error Estimation

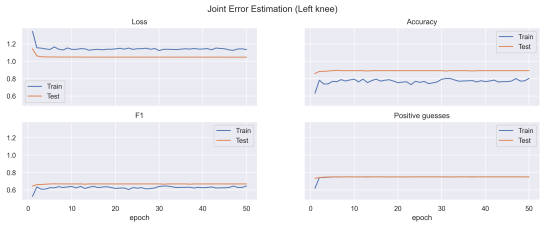

(a) left Knee Error Estimation

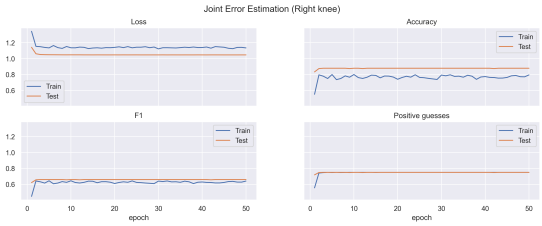

(b) Right Knee Error Estimation

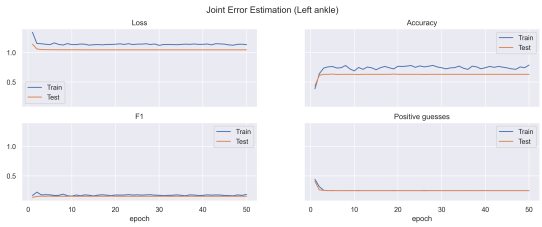

(c) Left Ankle Error Estimation

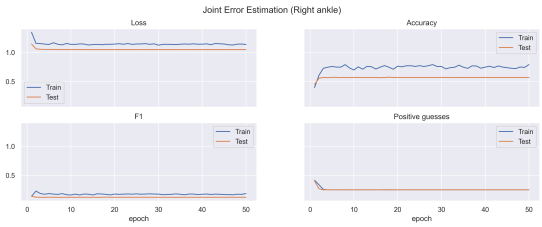

(d) Right Ankle Error Estimation

Figure C-9: The training results of the Joint error estimation model for FESDModelv1.

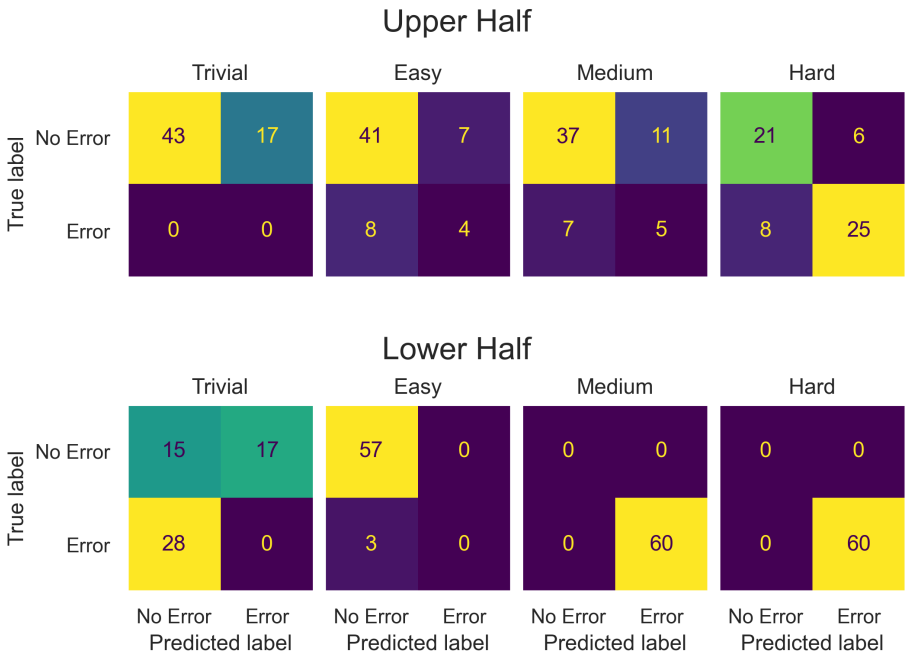

Figure C-10: The confusion matrix of the half body model by body half.

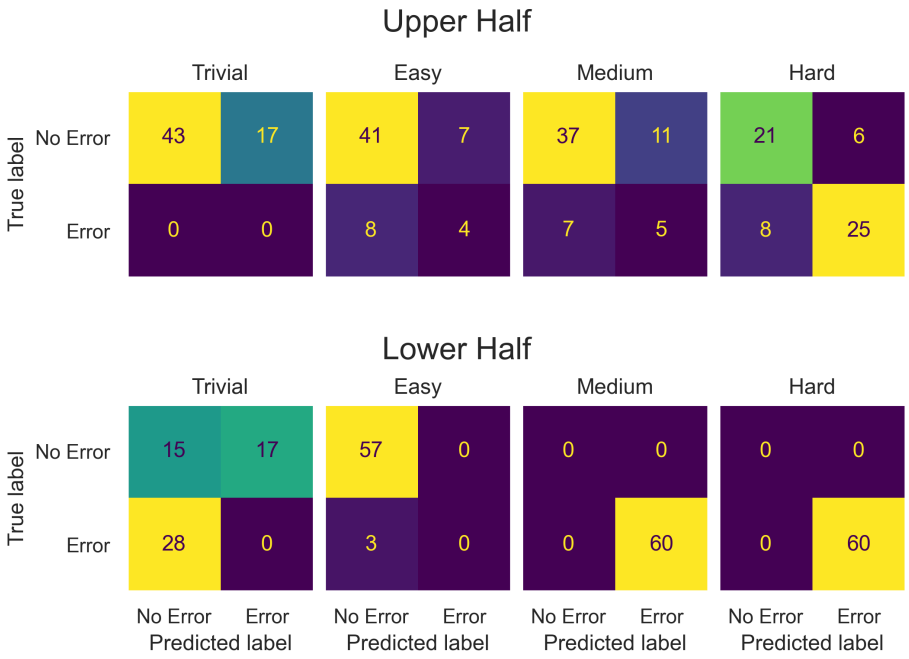

Figure C-11: The confusion matrix of the half body model by body half.

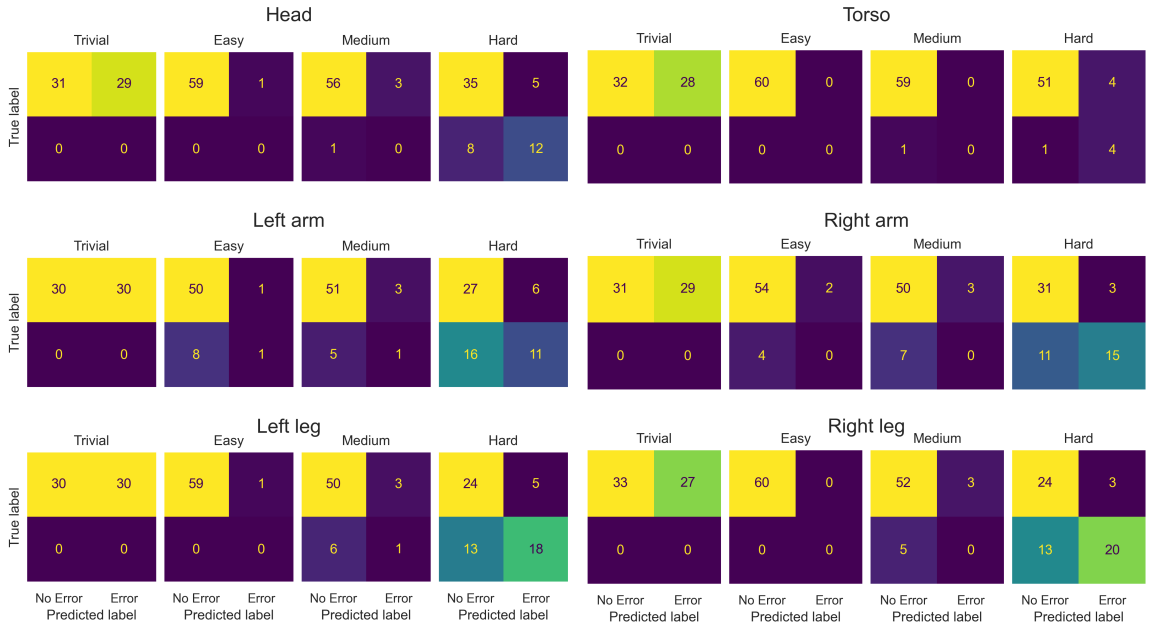

Figure C-12: The confusion matrix of the body part model by body half.

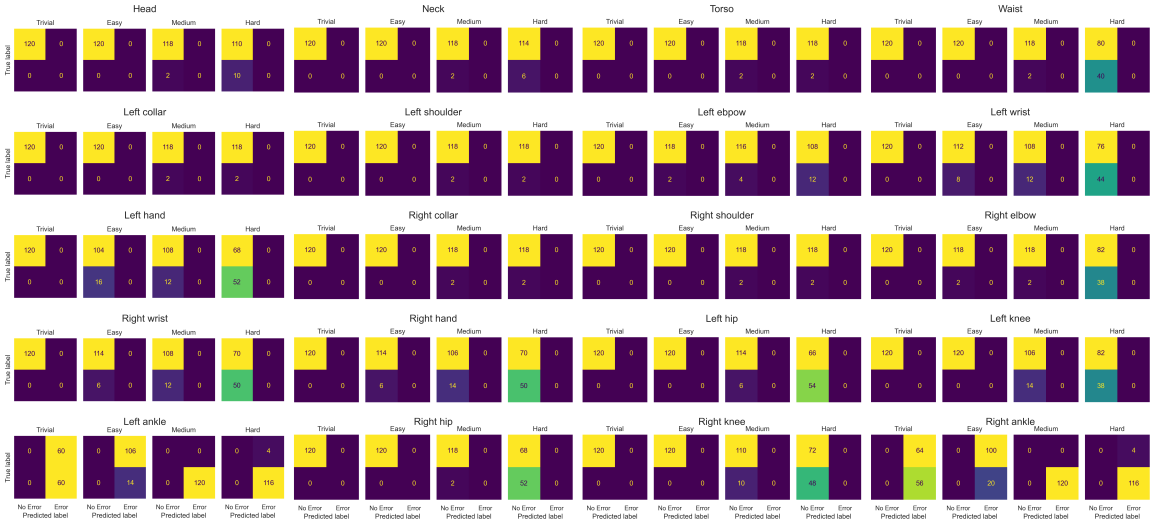

Figure C-13: The confusion matrix of the joint model by joint.

Appendix D

Additional Results for FESDModelv2

Figure D-1: The training results of the full body model.

(a) Upper Body Error Estimation

(b) Lower Body Error Estimation

Figure D-2: The training results of the half body error estimation model.

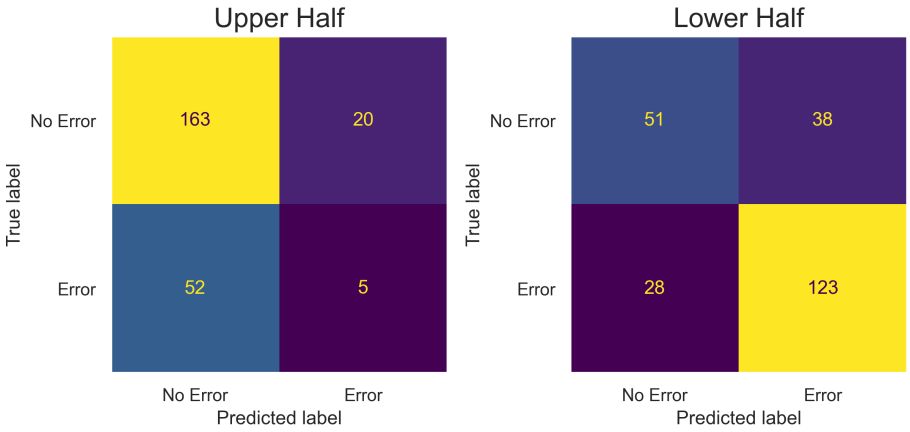

Figure D-3: The confusion matrix of the half body model by body half.

(a) Head Error Estimation

(b) Torso Error Estimation

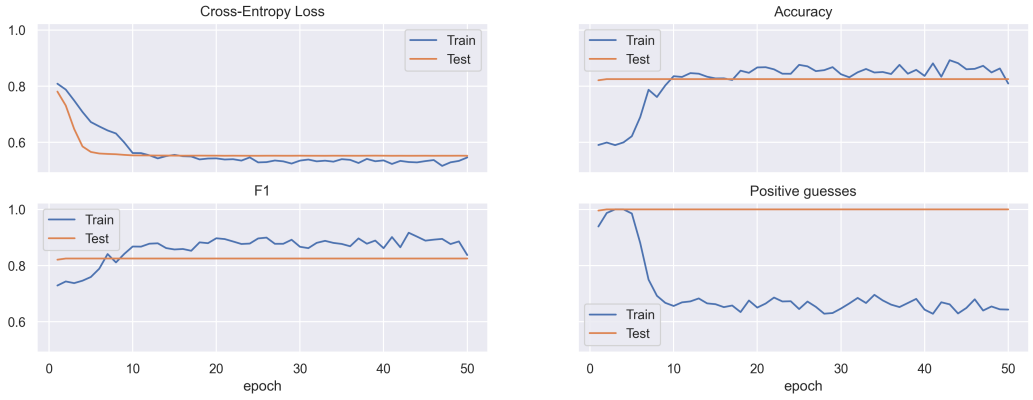

(c) Left Arm Error Estimation

(a) Right Arm Error Estimation

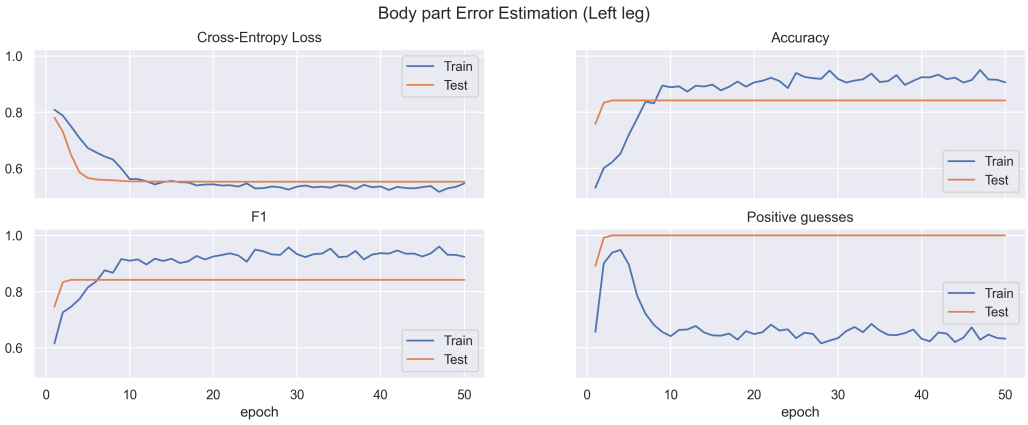

(b) Left leg Error Estimation

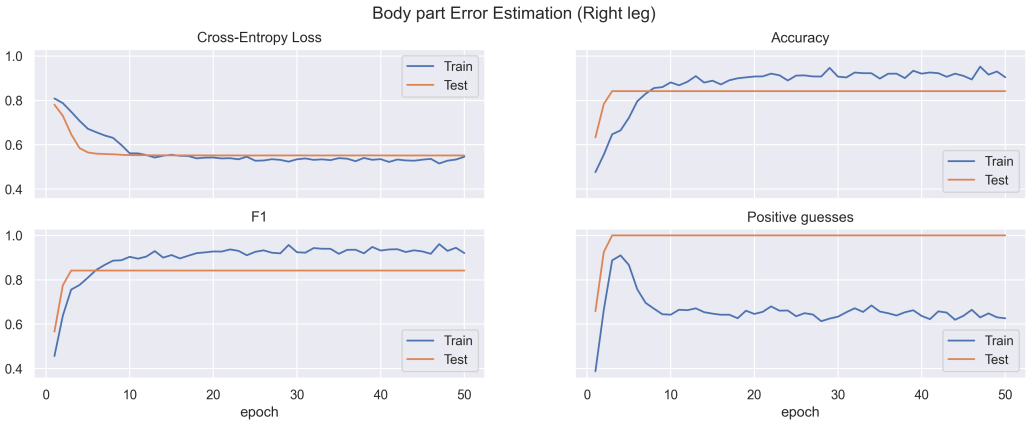

(c) Right leg Error Estimation

Figure D-5: The training results of the body part error estimation model.

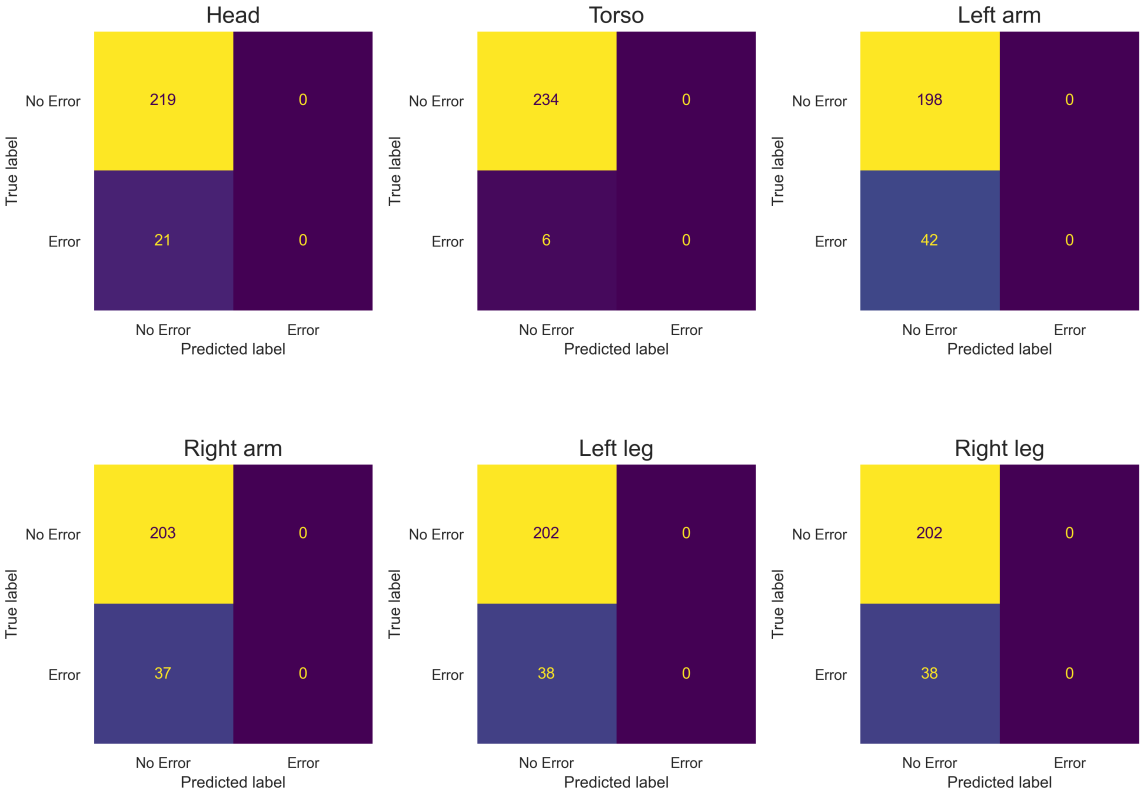

Figure D-6: The confusion matrix of the body part model by body part.

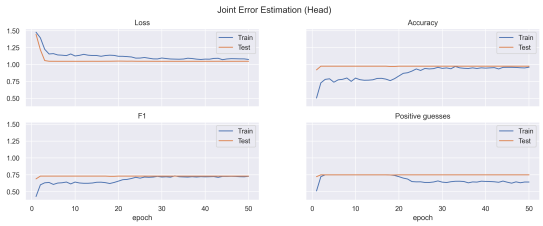

(a) Head Error Estimation

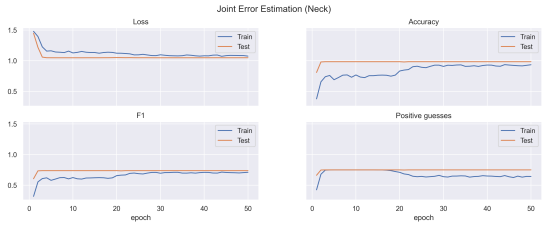

(b) Neck Error Estimation

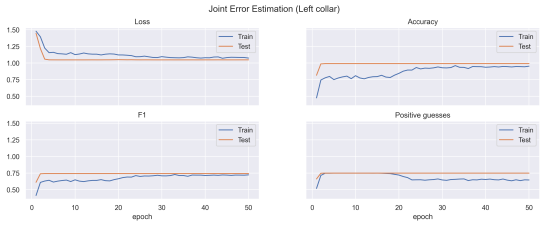

(c) Left Collar Error Estimation

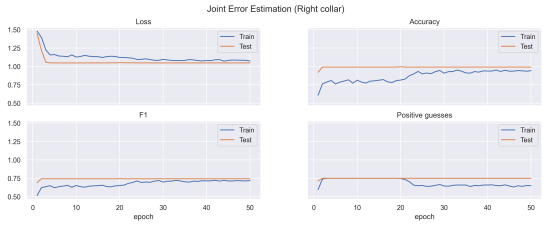

(d) Right Collar Error Estimation

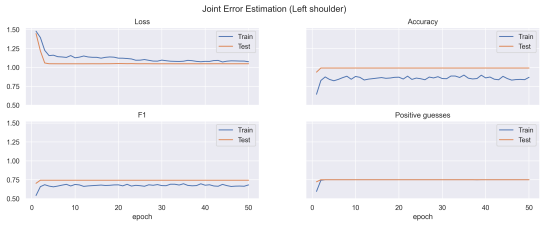

(a) Left Shoulder Error Estimation

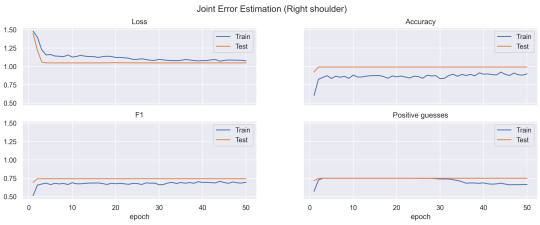

(b) Right Shoulder Error Estimation

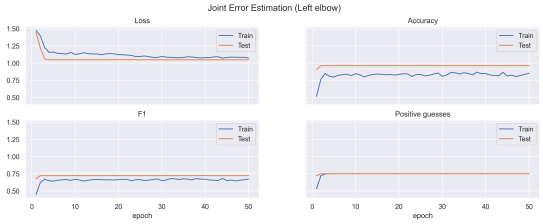

(c) Left Elbow Error Estimation

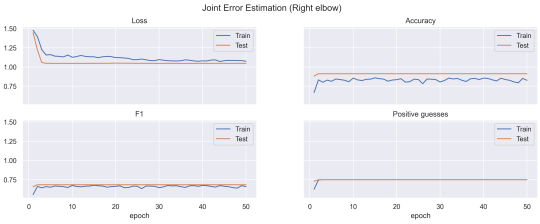

(d) Right Elbow Error Estimation

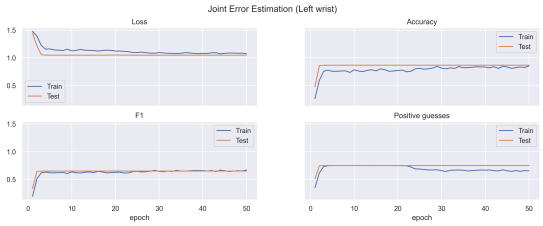

(a) Left Wrist Error Estimation

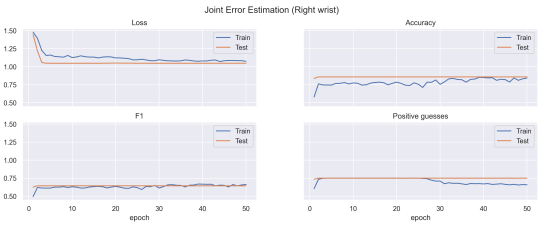

(b) Right Wrist Error Estimation

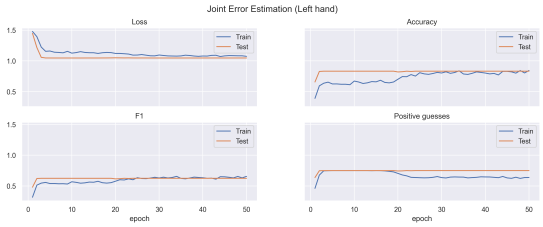

(c) Left Hand Error Estimation

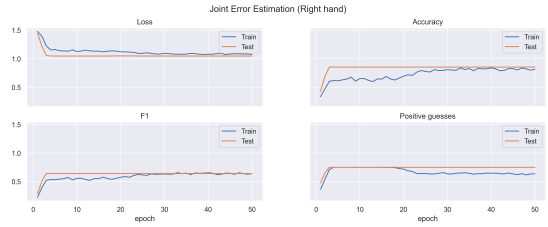

(d) Left Arm Error Estimation

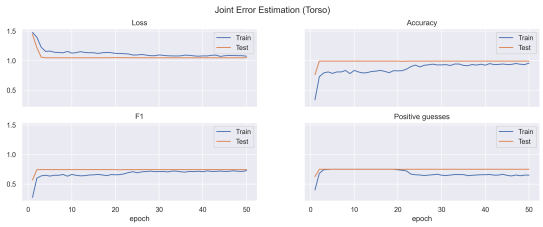

(a) Torso Error Estimation

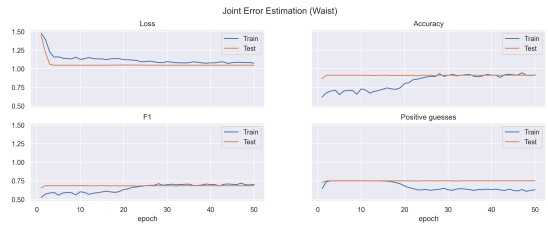

(b) Waist Error Estimation

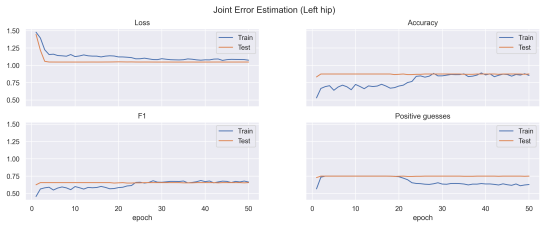

(c) Left Hip Error Estimation

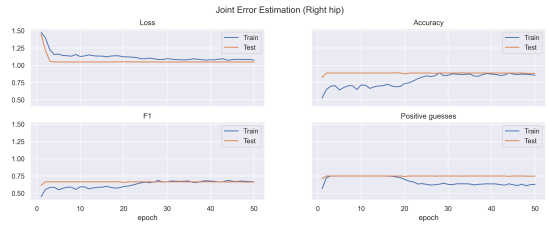

(d) Right hip Error Estimation

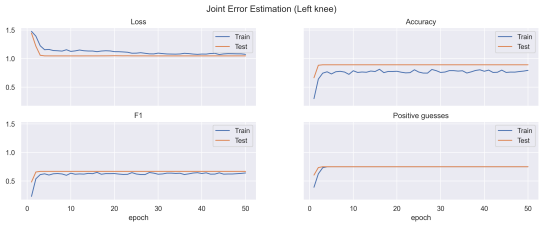

(a) left Knee Error Estimation

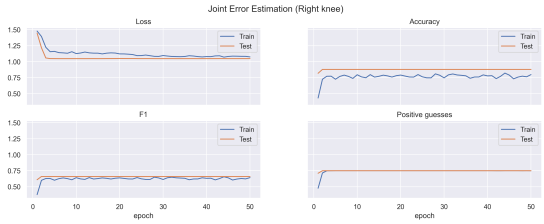

(b) Right Knee Error Estimation

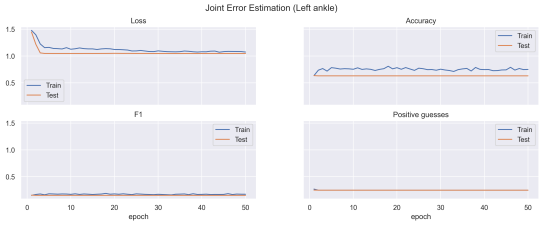

(c) Left Ankle Error Estimation

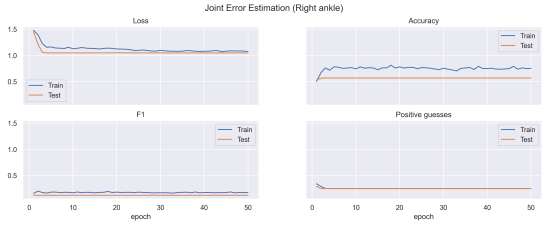

(d) Right Ankle Error Estimation

Figure D-11: The training results of the Joint error estimation model for FESDModelv2.

Figure D-12: The confusion matrix of the joint model by joint.